Journal of Bioprocessing & Biotechniques

Wensel, et al. J Bioproces Biotechniq 2011, S:2
DOI: 10.4172/2155-9821.S2-002

Research Article Open Access

Simulation with Computational Fluid Dynamics of Succinic Acid and Co-Product Biorefinery Process

Pierre Wensel, Liang Yu and Shulin Chen*

Department of Biological Systems Engineering, Washington State University, Pullman, WA 99164,USA

Abstract

Succinic acid is a di-carboxylic acid with tremendous future market potential, and there is increasing interest to produce it from microorganisms using cheap renewable resources like biomass. However, commercialization of bio-succinic acid is currently challenged by limited profitability of processes devoted solely to succinic acid, high downstream process costs, and minimal available industrial-scale simulation. To address these limitations, a novel industrial-scale biorefinery process to convert corn-stover into succinic acid and co-products was simulated using an integrated mathematical model developed from reported laboratory-scale experimental data. The upstream section of the biorefinery featured handling, pre-treatment, conversion, and separation of corn stover feedstock into a liquid fraction for ethanol processing and a solids fraction containing mostly cellulose that was further hydrolyzed into glucose for succinic acid processing. Subsequent units of operation were then simulated for a baseline process: Microfiltration was used to remove residual insoluble lignin, and glucose was then continuously fermented by the strain *M. Succiniciproducens MBEL55E* to produce succinate and by-products acetate, lactate, and formate. Additional steps to recover and purify succinic acid included cell microfiltration for cell removal, moving-bed adsorption for sugar removal and decolorization, nanofiltration for separation of succinate primarily from other salts, ion exchange for acidification and purification, and finally crystallization. The finite volume method of Computational Fluid Dynamics (CFD) was coupled with kinetic, stochiometric, mass, and energy balance equations to simulate the effects of inlet temperature impeller speed, diameter, and spacing, as well as inlet temperature and fermentor volume, on fermentor cooling jacket heat transfer area. Predicted dissolved CO_2 concentrations in the fermentor were in agreement with those in literature. The effects of microfiltration recirculation rate, microfiltration stage numbers, and adsorber sorbent particle diameter on dimensional requirements and power consumption were additionally evaluated. Yields and estimated volume and area requirements for units of operation were obtained for the baseline process and for those involving the simulated variable changes. This work represents the first reported industrial-scale bio-succinic acid process model.

Key words: Succinic acid; Biorefinery; Manheima succiniciproducens; Process simulation

Introduction

Succinic acid is a di-carboxylic acid which can be used as a C4 chemical building-block for manufacturing industrially valuable chemicals like adipic acid, N-methyl pyrrolidinone, 2-pyrrolidinone, succinate salts, 1,4-butanediol, maleic anhydride, tetrahydrofuran and gamma-butyrolactone, as well as ion-chelators, surfactants, detergents, synthetic resins, biodegradable polymers, pharmaceuticals, antimicrobials, food acidualants, flavor-enhancers, and green solvents [1-3]. Current succinic acid production ranges from 25,000–36,000 t/year, and market price ranges from $5.90–9.00(U.S.)/kg depending on purity [3, 4]. Succinic acid market and price were predicted to range from 180,000-27,000,000 t/year [1, 5], and from $0.50- 1.50(U.S.)/kg, respectively [2, 5].

Conventional production of succinic acid involves chemically processing fossil-based resources like petroleum through oxidation of n-butane or benzene via maleic anhydride, followed by hydrolysis and dehydrogenation [2, 6]. However, there is increased commercial and scientific interest to instead produce succinic acid from microorganisms using cheaper renewable resources like biomass. In 2004, the U.S. Department of Energy designated succinic acid as one of the top value-added chemicals from biomass [7]. Prospects of global bio-based succinic acid markets motivated companies Bioamber, DSM and Roquette, BASF and CSM, and Myriant to announce construction of new plants since 2010 [8-10]. We previously demonstrated a process involving pre-treatment and hydrolysis of inexpensive and renewable ligno-cellulosic waste and residue like corncob from agricultural and food industries to yield substrates for microbial fermentative production of succinic acid and co-products [11].

Commercialization of bio-succinic acid is nonetheless currently challenged by limited profitability when a plant is devoted solely to succinic acid [5]. Succinic acid production should therefore occur in an integrated biorefinery, where co-production of ethanol, other carboxylic acids, and on-site steam and electricity via processing of recovered lignin residues enhance profitability. Commercialization is also challenged by high downstream costs associated with isolation, purification, and sterilization of end-products accounting for up to 80% of total production cost [12]. For example, succinic acid precipitation by Ca^{2+}-containing species results in excessive sludge waste and also adversely affects the fermented cellular metabolism and cell membrane fluidity and permeability [12-14]. Reactive extraction with tri-n-octalamine (TOA) [15] can remove glucose but suffers from organic solvent toxicity and waste. A promising batch laboratory-scale process involving four-acid products *Actinobacillus succinogenes* fermentation and downstream centrifugation, filtration, activated carbon adsorption, cation-exchange chromatography, vacuum distillation, crystallization, filtra-

***Corresponding author:** Shulin Chen, Department of Biological Systems Engineering, Washington State University, Pullman, WA 99164, USA, Tel: 509-335-3743; Fax: 509-335-2722; E-mail: chens@wsu.edu

Received November 01, 2011; **Accepted** December 08, 2011; **Published** December 10, 2011

Citation: Wensel P, Yu L, Chen S (2011) Simulation with Computational Fluid Dynamics of Succinic Acid and Co-Product Biorefinery Process. J Bioprocess Biotechniq S2:002 doi:10.4172/2155-9821.S2-002

tion, and drying achieved an 89.5% succinic acid yield from substrate and 99% purity [8]. However, a commercial-scale biorefinery should instead recover valuable and volatile pyruvic, acetic, and formic acid by-products rather than eliminate them at 60°C and pH 4 with vacuum distillation [16]. In contrast, a nanofiltration process achieved sharp and non-destructive separation of succinate from a quartenary mixture containing lactate as opposed to pyruvate co-product but was not integrated with other purification steps [17].

Electrodialysis has been effectively used to concentrate and acidify succinic acid and other organic acids due to its environmental benignity, scalability, and ability to achieve high purity [18-27]. For instance, de-salting electrodialysis removed impurities and achieved a suitably concentrated, but undersaturated (< 25% weight) succinate solution for one process [22]. This was then converted into a supersaturated succinic acid solution where ionized succinic acid was converted into undissociated succinic acid by passing it through a water-splitting bipolar electrodialysis unit, from which an alkali NaOH stream was recycled to neutralize produced acids [22].Conventional electrodialysis was similarly integrated to a feed containing concentrated organic salt sodium gluconate to a bipolar membrane as a way to increase stability and limit a decrease in current efficiency and dramatic increase in energy consumption that frequently results at a high organic salts conversion rate in bipolar membranes due to salt depletion in feed compartments and organic acids diffusion [25]. Integration resulted in an apparent current efficiency higher than 100%, low energy consumption, and a predicted process cost of \$0.31 kg^{-1}, which was less than the \$0.39 kg^{-1} for the bipolar membrane [25]. Another process involving a succinic acid fermentation by *E.coli* strain ATCC202021 used first nanofiltration and then desalting electrodialysis to further concentrate and purify succinate salts and remove small and large molecular weight nonionic or weakly ionic compounds like sugars [26]. Severe membrane fouling was here alleviated by cleaning-in-place, reducing protein content in the fermentation broth, and raising its pH prior to microfiltration to denature the majority of proteins [26]. A mono-polar electrodialysis unit was also integrated with a continuous cell recycle fermentor for the production of succinic acid by *A. succinogenes* to continuously remove succinate and acetate from the permeate and recycle an organic acids-depleted solution back to the fermentor [19]. Compared to the cell recycle fermentor, this resulted in a five-fold increase in succinate concentration to 83 g/L at a high average succinate yield of 1.35 mol/mol and a slightly lower volumetric productivity of 10.4 g/ L^{-1} h^{-1}[19].

Nonetheless, a comparison between the technical feasibility of electrodialysis and that of other downstream methods must consider various factors like the cost of membrane and electrical energy consumption [8, 13, 18]. This may depend on purity levels and concentration profile, which in turn depends on water transport, the co-ion leakages through homopolar membranes, and the current density [28]. Also, to achieve higher succinic product fermentation concentrations than those obtained with NaOH, $MgCO_3$ has not only been used as a (1) pH controlling alkaline neutralizer to prevent acid product inhibition, but also as (2) a more soluble source of inorganic carbon than CO_2 gas requiring expensive compression, and (3) as a source of the co-factor Mg^{2+} for the enzyme PEP carboxykinase that is essential for succinate synthesis [14]. The inability of downstream electrodialysis membranes for acidification and purification to effectively handle divalent Mg^{2+} cation-containing species was therefore considered a major limitation [2]. Exploitation of the Donnan charge exclusion and the fixed charges of most nanofiltration membranes was also deemed more appropriate than electrodialysis when separating ionic by-product organic acid salts from succinate and when separating salts from organic electrolytes typically present in effluents produced by salt-generating reactions or by acid- or alkali-generating reactions followed by neutralization [17, 27]. Furthermore, the process costs and competitiveness of using either electrodialysis with bipolar membrane or ion exchange to acidify the carboxylic glucamonic acid were theoretically calculated by introducing two factors for environmental pollution and bipolar membrane prices and then compared [18]. Although these processes could be integrated to reduce environmental factors, results indicated that total process cost for ion-exchange was \$0.057 kg^{-1} and less than that for bipolar membrane electrodialysis (\$0.085–0.407 kg^{-1}) [18].

There is also limited reported industrial-scale process simulation and economic analysis for bio-succinic acid fermentation, recovery, and purification [29]. For instance, experimentally-derived succinic acid crystal growth and nucleation kinetics [30], succinic acid and lactic acid liquid-solid sorbent equilibria [31], and rejection coefficients at specified transmembrane pressure and flux [17] were not then used to simulate integrated large-scale crystallizers, ion exchangers, or nanofilters, respectively. Model-predicted CO_2 solubility and its experimentally observed effects on growth and succinic acid production during *M. succiniciproducens* fermentation were reported [32]. Kinetics for growth, glucose consumption, carboxylic acid production, and product and substrate inhibition were also simulated and experimentally verified for small-scale batch *M. succiniciproducens MBEL55E* [6] and *A. succinogenes* [33] fermentations. However, a robust commercial-scale process model should involve continuous fermentors since their productivity will be at least 5.3 times greater than that of batch fermentors [34]. A continuous fermentor integrated with monopolar electrodialysis membrane for removal of cells and inhibitory levels of acetate and lactate was reported but not modeled [19].

A robust commercial-scale process model should also account for hydrodynamic phenomena in a continuous fermentor and its impact on heat and mass transfer, temperature and nutrient uniformity, and, when applicable, cell shear-sensitivity. For instance, growth inhibition of *M. succiniciproducens MBEL55E* was observed beyond an accumulated carboxylic acid concentration of 17.23 kg/m^3 in a small 5-L batch fermentor [6]. Growth inhibition was also observed below a dissolved CO_2 concentration of 8.74 mM in a small 6.6-L batch *M. succiniciproducens* fermentor [32]. Overcoming these pilot-scale limitations at more heterogeneous commercial scales via, for instance, addition of neutralizing $MgCO_3$ base and carbon source and higher inlet CO_2 partial pressures and agitation impeller speeds will be more systematically achieved by feeding and sparging strategies derived from hydrodynamic studies characterizing mixing times and gas-liquid mass transfer coefficients.

We here describe and simulate a novel commercial-scale succinic acid biorefinery process featuring upstream corn-stover pre-treatment, hydrolysis, and cross-flow microfiltration and centrifugation for lignin recovery to yield sugars both for a co-ethanol fermentation and continuous *M. succiniciproducens* glucose fermentation for succinic acid, lactic, acetic, and formic acids production. These are then recoverable by microfiltration for cell removal, adsorption for decolorization and glucose removal, nanofiltration for non-destructive separation of succinate, ion exchange chromatography, crystallization, filtration, and drying. A baseline process was assumed, but the effects of microfiltration recirculation rate, microfiltration stage numbers, fermentation productivity kinetics, and adsorber sorbent particle diameter on dimensional requirements and power consumption for capital and operating cost estimation were simulated. Effects of impeller speed and inlet temperature on fermentor power and cooling jacket heat transfer area were also simulated by coupling mass and energy balances and experimentally-

derived kinetics to the finite volume method of Computational Fluid Dynamics (CFD).

CFD involves numerical solution of conservation equations for mass, momentum and energy in a flow geometry of interest, together with additional subsidiary sets of equations reflecting the considered problem [35]. Flow optimization via this tool represents significant potential savings in time and resources and increased profitability for a low profit margin, bio-commodity succinic acid process [35] by providing more data than physical trials and reducing the need for numerous and expensive experiments with prototype fermentors and probes. This is the first reported process simulation for industrial-scale bio-succinic acid production.

Method

Microsoft Excel v. 2007 software was used for calculations associated with process mass and energy balances, unit simulation via variable changes, and cost and sensitivity analysis. CFD numerical procedure was conducted with commercial code FLUENT (v.6.3.26)[36]. The simulated biorefinery process is shown (Figure 1). Description of major process streams are listed (Table 1). The feedstock was corn stover containing approximately 40–45% cellulose, 30–35% hemicellulose, and 10–20% lignin [11].The biorefinery was located in Iowa, a state accounting for 19% of total U.S. corn production having infrastructure to fulfill biorefinery requirement for co-production of corn-based ethanol. Capacity of 2,500 tons (wet basis) of corn stover/day was selected according to a National Renewable Energy Laboratory (NREL) model where raw material was collected within a 50 km radius [37]. This was the basis for the mass and energy balances and flow rates to simulate the succinic acid process units ranging from lignin microfiltration to crystallization. Unlike for plants devoted solely to ethanol fuel production, the generalized energy balance did not aim to show the extent that corn stover was converted into fuel energy since acid products were not fuels. Instead, energy losses and stream energy content were estimated:

$$E_{stover} = E_{electricity} + E_{ethanol} + E_{lactic\ acid} + E_{acetic\ acid} + E_{formic\ acid} + E_{succinic\ acid} + E_{steam+hot\ water} \quad (1)$$

Energy content was determined by multiplying mass flux by the corresponding High Heating Values (HHV) of 16, 29.7, 21.1, and 32.1 MJ/kg for corn stover, ethanol, lignin, and for each of the carboxylic acid products, respectively [38]. Electricity requirement was determined from estimates of electrical motor power consumption (i.e. for fermentor and crystallizer agitator), control systems, etc. Thermal energy requirement was determined from individual unit energy balances.

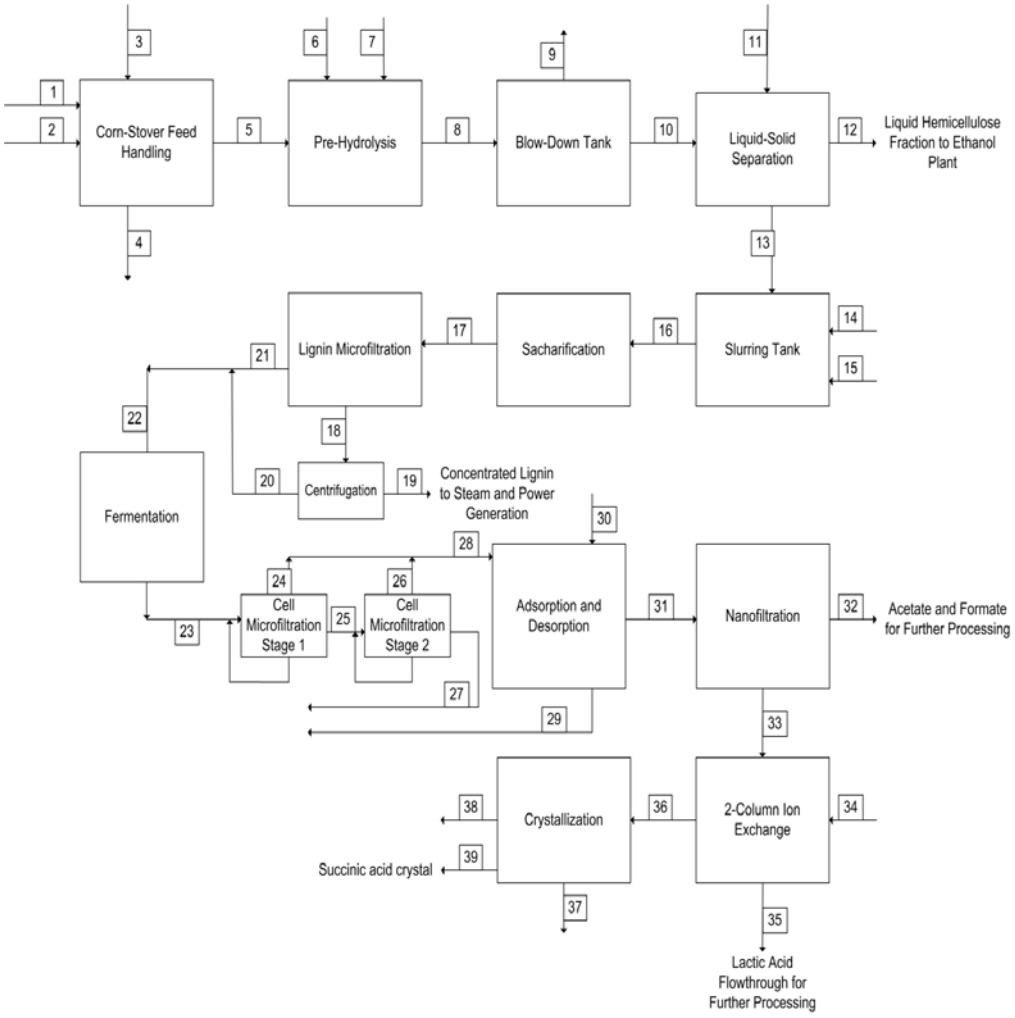

Figure 1: General flow diagram for succinic acid biorefinery.

Major Process Stream ID	Description
1	Corn Stover Feedstock (Dry Basis)
2	Corn Stover Feedstock Water Moisture Content
3	Losses
4	Supplemented Water
5	Shredded Corn Stover
6	Sulfuric Acid
7	Steam
8	Pre-treated Stover 1
9	Steam
10	Pre-treated Stover 2
11	Supplemented Water
12	Liquid Hemicellulose Fraction to Ethanol Plant
13	Solids Cellulose Fraction to Succinic Acid Plant
14	Calcium Hydroxide
15	Supplemented Water
16	Cellulose Fraction to Sacharification
17	Hydrolysate
18	Lignin Microfiltration Retentate
19	Concentrated Lignin to Steam and Power Generation
20	Centrifuged Retentate Flowthrough
21	Lignin Microfiltration Permeate
22	Combined Permeate Feed to Fermentation
23	Fermentation Product Streams (Cells, succinate, acetate, formate, and lactate)
24	Cell Microfiltration Stage#1 Permeate
25	Cell Microfiltration Stage#2 Retentate
26	Cell Microfiltration Stage#1 Permeate
27	Cell Microfiltration Stage#2 Retentate
28	Combined Permeate Feed to Adsorption and Desorption
29	Recovered Glucose Sugars
30	Regenerating Hot Water Solution
31	Nanofiltration Feed
32	Nanofiltration Permeate
33	Nanofiltration Retentate
34	Hot Water Regeneration Solution
35	Lactic Acid Flowthrough for Further Processing
36	Stripped Lactic Acid Eluant
37	Vented Water Vapor
38	Mother Liquor from Circulating Magma for Further processing
39	Succinic Acid Crystal

Table 1: Description of major process flow streams.

Upstream processes including lignin microfiltration and centrifugation

Upstream processes ranging from raw material corn stover feed handling to sacharification resembled those of a previous corn-based ethanol biorefinery [37], with the following major modifications and simplifying assumptions: First, pre-hydrolysis, the most thermal energy-consuming plant process, involved 1.2% diluted sulfuric acid and pressurized steam at 245°C, and 13.6 bar instead of ammonia fiber expansion (AFEX) to enable separation of liquid hemicellulose streams composed primarily of pentoses for ethanol fermentation and solid cellulose streams composed primarily of hexoses for glucose-based succinic acid fermentation. Second, the process included single-stage cross-flow tubular microfiltration units and centrifuge to remove and recover insoluble lignin from hydrolysate for combustion in a boiler and extra biorefinery steam and electricity.

Lignin-generated steam flow rate was calculated from lignin HHV, a boiler thermal efficiency of 0.65, specific enthalpy of steam at pre-hydrolysis conditions, and recovered lignin flow rate. For microfiltration, all insoluble lignin was retained, and the amount of glucose substrate partitioned to the retentate and permeate was 5% and 95% by mass, respectively. Retentate lignin concentration was specified based on a reported level 300g/L of soluble lignin ultra-filtered in a pulp and mill plant [39]. To avoid rapid membrane caking or fouling, recirculation rate of 6m/s was used for the baseline process but also varied for simulation, and specified inner diameter and length dimensions of the tubular module ensured turbulent Reynold's number. Assuming 40μm diameter spherical and insoluble lignin particles, inertial-lift theory [40] was used to calculate constant critical permeate flux representing 66% of the steady-state permeate flux [41] as follows:

$$J_c = \frac{0.024 \rho_p r^3 \gamma^2_w}{\mu_p} \quad (2)$$

where J_c is critical permeate flux (m/s), ρ_p is permeate density (kg/m^3), μ_p is permeate viscosity (Pa*s), r is lignin particle radius (m), and γ_w is tubular wall shear rate (s^{-1}). Microfiltration membrane area requirement was the ratio of mass balance-derived permeate flow rate to critical flux. Microfiltration power consumption was calculated [42]:

$$P_{micro-1} = \frac{0.04\,\mathrm{Re}^{-0.25} A_{micro-1} U^3_{micro-1} \rho_p}{\eta_p} \quad (3)$$

where $P_{micro-1}$ is pump power consumption (J/s), $U_{micro-1}$ is recirculation rate (m/s), η_p is pump efficiency (Dimensionless), $A_{micro-1}$ is the area requirement (m^2), and Re is Reynold's Number (Dimensionless) calculated as follows:

$$\mathrm{Re} = \frac{U^3_{micro-1} d_{micro-1} \rho_p}{\mu_p} \quad (4)$$

Where $d_{micro-1}$ is tube inner diameter (m). The microfiltration retentate was then centrifuged to further de-water and concentrate its lignin prior to boiler combustion. A Sigma Factor Σ specifying disk-type centrifuge area requirement was calculated [40]

Fermentation

The centrifuged and de-lignified retentate liquid stream containing glucose was then combined with microfiltration permeate, sterilized and cooled in external heat exchanger, and introduced to the continuous fermentor for succinic acid and co-production of lactic acid, acetic acid, and formic acid. The baseline process used the available batch kinetic parameters of *M. succiniciproducens MBEL55E* [6], a gram-negative capnophilic bacterium isolated from bovine rumen [32]. Succinic acid is metabolically both an intermediate of the reductive TCA cycle and fermentative end product for this and other anaerobic and facultative microorganisms [32]. Some other strains [3] have reportedly higher succinic acid yields and titers than *M. succiniciproducens* (Table 2). Some even have the flexibility of C5 and C6 sugar uptake [11] and Simultaneous Sacharification and Fermentation (SSF) [43]. However, their parameters were either unreported or less usable because yield and production terms were convoluted into single terms [33]. Nonetheless, the effect of substituting in an *A. succinogenes* succinic acid productivity term on overall succinic acid yield was simulated.

An algorithm depicting the CFD-coupled model to predict the effect of impeller speed and inlet temperature on fermentor cooling jacket heat transfer area requirement is illustrated (Figure 2). To initially determine fermentor dimensions for such CFD simulation, an idealized Continuously Stirred Tank Reactor (CSTR) at steady-state

Microorganims	Y (g/g glc)	q_{succ} (g/gDCW/h)	r_{succ} (g/l/h)	Titer (g/l)	Residence-Time (h)
C. glutamicum	0.92	0.06	3.17	146	46
A. succinogenes	0.82	N.D.	1.36	105.8	78
M. succiniciproducens	0.76	0.72	1.80	52.4	30

Table 2: Yields, reaction rates, and titers for *C. glutamicum, A. succinogenes, and M. succiniciproducens*.

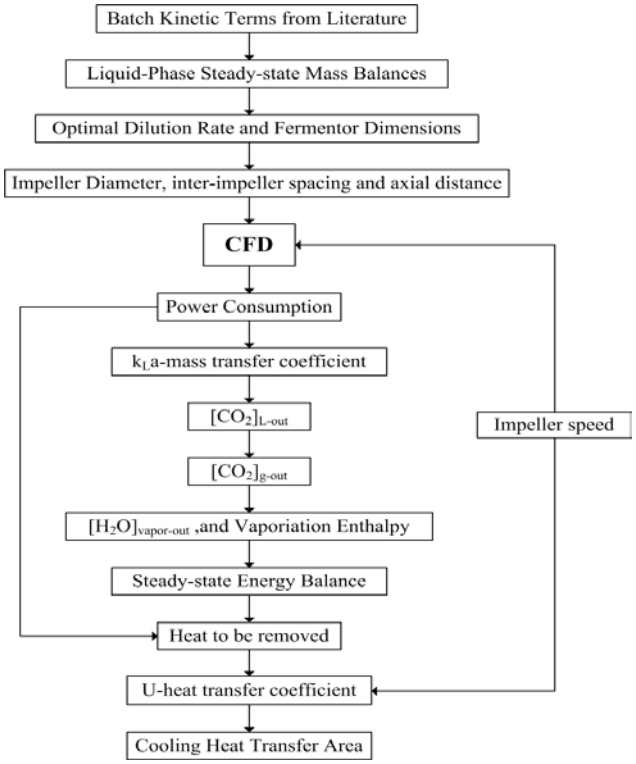

Figure 2: Algorithm of coupled CFD fermentor simulation.

with equivalent inlet and outlet flow rates was assumed. The fermentor was assumed to be cylindrical, free of headspace and internals, and sparged at the bottom by pure CO_2 gas from a clean, filtered, and recycled exhaust waste stream integrated from biorefinery ethanol fermentors. Steady-state liquid-phase mass balances for the component cell biomass, substrate, and carboxylic acid products using the available batch kinetic parameters of *M. succiniciproducens MBEL55E* [6] were therefore developed:

Viable cell liquid-phase mass balance:

$$\frac{dX_{ss}}{dt} = 0 = \frac{F(X_0 - X_{ss})}{V_L} + \mu X_{ss} - k_d X_{ss} \tag{5}$$

where is steady-state cell biomass concentration (kg DCW/m^3), is initial feed cell biomass concentration (kg DCW/m^3), μ is specific growth rate (s^{-1}), F is inlet/outlet volumetric flow rate (m^3/s), V_L is fermentor liquid volume (m^3), and is specific death rate (s^{-1}). Omitting substrate and product inhibition terms [6] and assuming Monod kinetics to avoid multiple non-washout steady-states [34], was further expressed as:

$$\mu = \frac{\mu_{\max} S_{ss}}{K_S + S_{ss}} \tag{6}$$

where $\mu_{\max}$ is maximum specific growth rate (s^{-1}), is glucose substrate half-saturation constant(kg/m^3), and S_{SS} is steady-state glucose substrate concentration (kg/m^3). Because feed was previously sterilized, $X_o = 0$ kg/m^3. The recycle of cells back to the fermentor after downstream microfiltration recovery was for simplicity not simulated. A shear-dependent death rate term coupled with CFD simulation parameters was included as follows [44]:

$$k_d = \frac{cN_{impeller}^{2.25} d_{cell} D_{impeller}^{3.75}}{\nu_l^{1.25} V_L^{0.75}} \tag{7}$$

where $N_{impeller}$ is rotational impeller speed (rps), d_{cell} is equivalent diameter for rodococcal *M. succiniciproducens* (m), $D_{impeller}$ is impeller diameter (m), is dynamic viscosity (m^2/s), V_L is fermentor liquid volume (m^3), and c is cell-dependent death rate constant (m^3/s). However, $k_d \sim 0$, as *M. succiniciproducens*, unlike animal cells, likely had a very small death rate constant since *E.coli* were reportedly damaged only at shear rates exceeding 1250 Pa [45].

Carboxylic acids product liquid-phase mass balances:

$$\frac{dP_{SAss}}{dt} = 0 = \alpha_{SA}\mu X_{ss} + \beta_{SA} X_{ss} - \frac{F(P_{SAss})}{V_L} \tag{8}$$

$$\frac{dP_{AAss}}{dt} = 0 = \alpha_{AA}\mu X_{ss} + \beta_{AA} X_{ss} - \frac{F(P_{AAss})}{V_L} \tag{9}$$

$$\frac{dP_{LAss}}{dt} = 0 = \alpha_{LA}\mu X_{ss} + \beta_{LA} X_{ss} - \frac{F(P_{LAss})}{V_L} \tag{10}$$

$$\frac{dP_{FAss}}{dt} = 0 = \alpha_{FA}\mu X_{ss} + \beta_{FA} X_{ss} - \frac{F(P_{FAss})}{V_L} \tag{11}$$

where P_{SAss}, P_{AAss}, P_{LAss}, and P_{FAss} are steady-state concentrations of succinic acid, lactic acid, acetic acid, and formic acid concentrations, respectively (kg/m^3), α_{SA}, α_{AA}, α_{LA}, and α_{FA} are growth-associated productivity terms for succinic acid, acetic acid, lactic acid, and formic acid, respectively (kg/kg), $\beta_{SA}, \beta_{AA}, \beta_{LA}$ and β_{FA} are non-growth associated productivity terms for succinic acid, acetic acid, lactic acid, and formic acid, respectively (kg/kg).

Glucose substrate liquid-phase mass balance:

$$\frac{dS_{ss}}{dt} = 0 = \frac{F(S_0 - S_{ss})}{V_L} - \frac{\mu X_{ss}}{Y_{x/s}} - \frac{(\alpha_{SA}\mu X_{ss} + \beta_{SA} X_{ss})}{Y_{SA/s}} - \frac{(\alpha_{AA}\mu X_{ss} + \beta_{AA} X_{ss})}{Y_{AA/s}} - \frac{(\alpha_{LA}\mu X_{ss} + \beta_{LA} X_{ss})}{Y_{LA/s}} - \frac{(\alpha_{FA}\mu X_{ss} + \beta_{FA} X_{ss})}{Y_{FA/s}} - m_s X_{ss} \tag{12}$$

where S_0 is initial glucose substrate feed concentration (kg/m^3), m_s is glucose substrate maintenance term (kg/kg), $Y_{x/s}$ is yield coefficient of biomass from glucose substrate (kg/kg), $Y_{SA/s}$ $Y_{AA/s}$ $Y_{LA/s}$ $Y_{FA/s}$ are yield coefficients for succinic acid, acetic acid, lactic acid, and formic acid, respectively, from glucose substrate (kg/kg). The steady-state cell biomass balance by substitution became:

$$\mu = \frac{F}{V_L} = D \tag{13}$$

Where D is dilution rate (s^{-1}). Substituting this dilution rate into steady-state mass balances resulted in the following:

$$S_{ss} = \frac{DK_s}{\mu_m - D} \tag{14}$$

$$X_{ss} = \frac{D(S_0 - S_{ss})}{D\left(\left(\frac{1}{Y_{x/s}}\right) + \left(\frac{\alpha_{SA}}{Y_{SA/s}}\right) + \left(\frac{\alpha_{AA}}{Y_{AA/s}}\right) + \left(\frac{\alpha_{LA}}{Y_{LA/s}}\right) + \left(\frac{\alpha_{FA}}{Y_{FA/s}}\right)\right) + \left(\frac{\beta_{SA}}{Y_{SA/s}}\right) + \left(\frac{\beta_{AA}}{Y_{AA/s}}\right) + \left(\frac{\beta_{LA}}{Y_{LA/s}}\right) + \left(\frac{\beta_{FA}}{Y_{FA/s}}\right) + m_s\right)} \tag{15}$$

$$P_{SAss} = \alpha_{SA} X_{ss} + \frac{\beta_{SA} X_{ss}}{D} \tag{16}$$

$$P_{AAss} = \alpha_{AA} X_{ss} + \frac{\beta_{AA} X_{ss}}{D} \tag{17}$$

$$P_{LAss} = \alpha_{LA} X_{ss} + \frac{\beta_{LA} X_{ss}}{D} \quad (18)$$

$$P_{FAss} = \alpha_{FA} X_{ss} + \frac{\beta_{FA} X_{ss}}{D} \quad (19)$$

An additional steady-state equation for volumetric succinic acid productivity was included:

$$DP_{SAss} = \alpha_{SA} DX_{ss} + \frac{\beta_{SA} X_{ss}}{D} \quad (20)$$

The steady-states of Equation 14-20 were then plotted against dilution rate. Graphically determined optimal dilution rate corresponding to maximum steady-state volumetric productivity was used to obtain the steady-state outlet liquid-phase biomass, glucose, and carboxylic acid product concentrations. Optimal dilution rate was also obtainable by setting the derivative of steady-state volumetric productivity with respect to dilution rate to 0. The fermentor liquid volume specifying dimensions for the baseline process as well as the CFD simulation was the ratio of F to optimal dilution rate. A 3:1 liquid fermentor height to diameter ratio was then assumed:

$$D_T = \left(\frac{4V_L}{3\pi} \right)^{1/3} \quad (21)$$

where D_T is fermentor diameter (m). Single-phase flow for Newtonian fluid, a three-impeller, 6-blade Rushton-turbine agitator, and a uniform inter-impeller axial spacing and distance from the bottom [46] equal to impeller diameter which itself was a third of fermentor diameter were assumed for both the baseline process and CFD simulation. For the baseline process, 40°C inlet temperature and 200 rpm agitation speed was assumed. CFD was used to simulate the effect of inlet temperature at 40°C and 42°C and impeller speeds at a minimal value, 100rpm, and 200rpm on cooling jacket area. Minimal impeller speed was estimated as follows [34]:

$$N_0 = \left(1.22 + 1.25 \left(\frac{D_T}{D_{impeller}} \right) \right) \left(\frac{\sigma g}{\rho_f} \right)^{1/4} \quad (22)$$

where N_0 is minimum impeller speed (rps), σ is surface tension of fermentation broth (dyne/m) and ρ_f is fermentation broth density (kg/m^3).

In addition to this simulation, the CFD flow fields resulting from a smaller fermentor liquid volume and alternate impeller spacing [47] were visualized. For this the bottom, middle, and top impeller distance from the fermentor bottom were instead multiples of 0.166, 1.2, and 1.967 times the fermentor diameter. The multiple reference frame (MRF) model was applied until the flow fields in the stirred-tank fermentor converged to steady-state values. MRF involved a steady-state approach in which individual cell zones moved at different rotational speeds. The flow fields for zones with impellers were solved with MRF equations, whereas those with no moving parts were solved using stationary-frame equations. The CFD governing equations were provided in the FLUENT (v.6.3.26) documentation [36]. Among these were the continuity equations, momentum equations, and turbulence model equations used to calculate the fluctuations involving momentum. To predict the effects of inlet temperature and impeller speed, non-aerated agitator power consumption was calculated by CFD as follows:

$$P_{impeller0} = 2\pi N_{impeller} M \quad (23)$$

where $P_{impeller0}$ is non-aerated impeller power consumption (W), and M is torque (moment) on the axis due to the impeller (N•m). Alternatively, a dimensionless power number N_p could be determined graphically from a Reynold's Number to estimate non-aerated power consumption as follows: [44]

$$\mathrm{Re}_p = \frac{N_{impeller} D_{impeller}^{\ 2} \rho_f}{\mu_f} \quad (24)$$

where μ_f is fermentation broth dynamic viscosity and [44]:

$$P_{impeller0} = N_p \rho_f N_{impeller}^{\ 3} D_{impeller}^{\ 5} \quad (25)$$

The Finite Volume Method (FVM) was the CFD numerical solution technique used since it accommodated unstructured meshes and was based on fundamental laws of conservation [48]. The continuity and momentum equations were discretized into algebraic equations and then solved numerically. The SIMPLE algorithm was used to solve velocity-pressure coupled differential equations. No-slip boundary conditions were applied on all walls. The wall temperature was set at the fermentation broth temperature 39°C [6]. The convergence criteria required that the scaled residuals decrease to 10^{-5} for each conservative equation. For gas-liquid two-phase flow where Re>10,000, mixing time (s) was estimated as follows [44]:

$$t_m = \frac{6 \left(\frac{D_T}{D_{impeller}} \right)^3}{N_{impeller} N_p^{0.33}} \quad (26)$$

Aerated power consumption $P_{impeller\,g}$ was then calculated [44]:

$$\frac{P_{impeller\,g}}{P_{impeller0}} = 0.10 \left(\frac{F_g}{N_{impeller} V_L} \right)^{-0.25} \left(\frac{N_{impeller}^{\ 2} D_{impeller}^{\ 4}}{g H_{impeller} V_L^{\ 2/3}} \right)^{-0.20} \quad (27)$$

where F_g is volumetric CO_2 gas flow rate (m^3/s), g is gravitational constant (m^2/s), and $H_{impeller}$ is height of impeller blade (m). The rate F_g was obtained from V_L and the 0.25 vvm of pure CO_2 reportedly sparged in *M. succiniciproducens MBEL55E* fermentation [6]. A superficial CO_2 gas velocity v_g (m/s) was obtained from F_g and D_T, and a volumetric gas-liquid mass transfer coefficient $k_L a$ (s^{-1}) was calculated from an empirical correlation for non-coalescing (dirty) dispersions as follows [34]:

$$k_L a = 0.002 \left(\frac{P_{impeller\,g}}{V_L} \right)^{0.7} v_g^{\ 0.2} \quad (28)$$

Using the CFD-derived $k_L a$, the steady-state CO_2 liquid-phase concentration exiting the fermentor $[CO_{2L}]_{ss}$ (kg/m^3) was then solved from the following steady-state mass balance:

CO_2 liquid-phase mass balance:

$$\frac{dV_L [CO_{2L}]_{ss}}{dt} = 0 = F_L \left([CO_{2L}]_0 - [CO_{2L}]_{ss} \right) + K_g a V_L P \left(y - \frac{H [CO_{2L}]_{ss}}{P} \right) - r_{co_2} V_L \quad (29)$$

where $[CO_2]_0$ is inlet CO_2 concentration (kg/m^3), y is CO_2 mass fraction in inlet gas sparging stream, H is Henry's Law constant (Pa kg CO_2 m^{-3}), P is total pressure (Pa), r_{co_2} is volumetric rate of consumption of CO_2 by reaction in the liquid phase (kg/s), and $K_g a$ is overall gas phase mass transfer coefficient (kgPa^{-1}s^{-1}). The Kga was approximated with $k_g a$ assumed negligible:

$$\frac{1}{K_g a} = \frac{1}{k_g a} + \frac{H}{k_L a} \quad (30)$$

It was assumed that there was no axial or time-dependence on the gas phase composition of the bubble since pure CO_2 was assumed sparged and y=1. Total pressure accounted for atmospheric and fermentor height-dependent hydrostatic pressure. CO_2 is incorporated in the PEP carboxylation pathway [32], and a reported 1:1 ratio of moles of CO_2 fixed to moles of succininc acid produced [6] was used for calculation of r_{co_2}. Metabolic production of CO_2 by *M. succiniciproducens* was not modeled [6]. The Henry's Law constant was adjusted for ionic

strength of fermentation broth using Bunsen coefficients [32]. The inlet liquid-phase concentration $[CO_2]_0$ was 0 kg/m^3.

Flow rates and solved $[CO_{2L}]_{ss}$ concentration and inlet gas-phase concentration $[CO_{2G}]_0$ were then used to calculate steady-state gas-phase CO_2 concentration $[CO_{2G}]_{ss}$ exiting the fermentor at the top (kg/m^3) from a total CO_2 fermentor mass balance. The mass fraction of water vapor also exiting the top was estimated from ratio of water vapor pressure estimated with the Antoine equation [49] at atmospheric pressure and 39°C to total atmospheric pressure. This and the exiting CO_2 gas mass flow rate $F_{CO2g-out}$ (kg/s) were then used to obtain a mass flow rate of exiting water vapor $F_{watervapor_{out}}$ (kg/s). With gas and liquid-phase mass flow rates now specified, a fermentor energy balance provided the heat removed term using the agitator power consumption and exiting CO_2 and water vapor enthalpy terms obtained from CFD simulation:

$$Q_{removed} = \eta_{impeller} P_{impeller\,g} + \sum_{i=1}^{n} F_{i_{in}} H_{i_{in}} - \sum_{i=1}^{n} F_{i_{out}} H_{i_{out}} \quad (31)$$

where $Q_{removed}$ is rate of heat to be removed (J/s), $\eta_{impeller}$ is gearbox efficiency, $F_{i_{in}}$ and $F_{i_{out}}$ are inlet and outlet mass flow rates of components i, respectively (kg/s), $H_{i_{in}}$ and $H_{i_{out}}$ are inlet and outlet mass enthalpy of components i, respectively (J/kg). With exception of terms for water vapor involving a phase change and *M. succiniciproducens* cells, component enthalpy terms were calculated as follows:

$$H_i = H_i^o(T_R) + \int_{T_R}^{T_2} C_{p_i} dT \quad (32)$$

where $H_i^o(T_R)$ is heat of combustion for component i (J/kg) at reference temperature T_R= 25°C, T_2 is fermentation broth temperature of 39°C for outlet streams and either the baseline 40°C or simulated 42°C for inlet liquid streams, and C_{p_i} is heat capacity of component i (J/kg-C). Water vapor mass enthalpy was similarly calculated but by also adding an enthothermic enthalpy of vaporization for water vapor (J/kg). Heat of combustion mass enthalpy for *M. succiniciproducens* cell biomass on dry-weight, 8% ash-basis was calculated by the Dulong equation [34]:

$$H_{cell}^o = 8.076C + 34.462(H - \frac{O}{8}) \quad (33)$$

where C, H, and O represent the experimentally-determined weight fractions of carbon, hydrogen, and oxygen, respectively, for *M. succiniciproducens* from its cell elemental composition $CH_{1.736}O_{0.367}N_{0.240}$ [6]. Assuming cooling water with inlet and outlet temperatures of 25°C and 35°C flowing through an external jacket having a small equivalent width of 0.0254 m, a high cooling water mass flow rate was obtained from $Q_{removed}$, temperature difference, and water heat capacity. Fermentor cooling jacket heat transfer area requirement was therefore calculated:

$$A_{heat} = \frac{Q_{removed}}{U(T_C - T_F)} \quad (34)$$

where U is overall heat transfer coefficient (W/m^2-C), T_C is average cooling water temperature of 30°C, and T_F is fermentation broth temperature of 39°C. Like the previous overall mass transfer coefficient $K_g a$, overall heat transfer coefficient was approximated as a sum of resistances in series as follows:

$$\frac{1}{U} = \frac{1}{h_F} + \frac{1}{h_{FD}} + \frac{\Delta x}{k_W} + \frac{1}{h_C} + \frac{1}{h_{CD}} \quad (35)$$

where h_F is heat transfer coefficient for the fermentation broth (W/m^2-C), h_{FD} is heat transfer coefficient (a.k.a. dirt factor) from fermentation broth fouling deposits (W/m^2-C), k_w is thermal conductivity of the fermentor wall stainless steel (J/m^2), Δx is fermentor wall thickness (m), h_c is cooling water heat transfer coefficient (W/m^2-C), and h_{CD} is cooling water fouling deposits heat transfer coefficient (W/m^2-C). The fermentation broth heat transfer coefficient h_F depended directly on impeller speed and diameter specified for CFD simulation as follows [34]:

$$\frac{h_F D_T}{k_F} = 0.42\left(\frac{D_{impeller}^{\ 2} N_{impeller} \rho_F}{\mu_F}\right)^{0.66}\left(\frac{C_{pF}\mu_F}{k_F}\right)^{0.33}\left(\frac{\mu_F}{\mu_W}\right)^{0.14} \quad (36)$$

where μ_W is wall viscosity (kg/s-m) and k_F is fermentation broth thermal conductivity (W/m-C). Effect of impeller speed and inlet temperature on heat transfer area was therefore simulated.

Cell microfiltration

A two-stage cross-flow tubular microfiltration unit, whereby the retentate of the first stage became the feed of the second stage, then removed and recovered all cells from the broth exiting the fermentor containing succinate, acetate, formate, lactate, and unconsumed glucose. The intended recycle of cells back to the fermentor for simplicity was not simulated. Final cell retentate concentration was limited to 100 kg/m3 because this corresponded to an exponential increase in viscosity and a non-Newtonian transition of a lactic acid fermentation broth increasing pump energy consumption [50]. For the mass balance, the permeate volumetric flow rate of the first stage was equal to that of the second stage, and inter-stage recycle ratio was equal to 1. All non-cell components in the feed transferred to the permeate because they were below the molecular weight cutoff of the microfiltration membrane. Recirculation rate was 6m/s. Steady-state permeate flux was estimated using a gel polarization model [51, 52]:

$$J_{micro-2} = 1.31\left(\frac{D_{cell}^{\ 2}\gamma}{L_{micro-2}}\right)^{1/3}\left(\frac{c_{gcell}}{c_{0cell}} - 1\right)^{1/3} \quad (37)$$

where D_{cell} is particle diffusion coefficient of *M. succiniciproducens* cells in succinic acid fermentation broth (m^2/s), $L_{micro-2}$ is tube length (m), γ is shear rate (s^{-1}), C_{gcell} is gel polarization volume fraction, and C_{ocell} is bulk cell volume fraction. Effect of single-stage on area and power requirements, calculated as before, was simulated and compared to two-stage baseline process.

Adsorption and desorption

A granulated activated carbon (GAC) counter-current moving-bed adsorber then removed 98% of glucose from microfiltration permeate to further purify the products. Intended recycle of glucose back to the fermentor for simplicity was not simulated. Only 2.5% lactate and 1% succinate was lost in the sorption process. GAC sorbent was selected for its low cost and future derivation from biochar via pyrolysis of recovered lignin. Column height was estimated from the product of NTU (Number of Transfer Units) and HTU (Height of Transfer Units).NTU was calculated by integrating area from a plot of the single-component glucose equilibrium curve and of the mass balance-derived operating line [53]. The adsorption equilibrium curve was generated from Langmuir single-component glucose-GAC equilibria isotherm data [54]:

$$q_{glu} = \frac{q_{m_{glu}} b C_{glu}}{1 + b C_{glu}} \quad (38)$$

where q_{glu} is glucose concentration in GAC sorbent phase (mol glucose/kg GAC sorbent), q_m is maximum sorbent capacity (mol glucose/kg GAC sorbent), C_{glu} is glucose concentration in liquid phase (mol glucose /m^3 feed solution). HTU was estimated as follows [53]:

$$HTU = \frac{v_{adsorber}}{K_{adsorber} a_i} \quad (39)$$

where $K_{adsorber}$ is overall mass transfer coefficient (m/s), $v_{adsorber}$ is industry-acceptable adsorber hydraulic loading rate based on selected

column diameter (m/s), and a_i is particle interfacial area/volume ratio (m^{-1}) calculated as follows:

$$a_i = \frac{6(1-\varepsilon)}{d_p} \quad (40)$$

where ε is bed porosity or void fraction (dimensionless) and d_p is GAC particle diameter(m), which for the baseline process was 800μm but was also simulated at 600μm. Overall mass transfer coefficient $K_{adsorber}$ was estimated as follows [55]:

$$\frac{1}{K_{adsorber}} = \frac{1}{k_{film}} + \frac{1}{q_m k_s} \quad (41)$$

where k_{film} is film-mass transfer coefficient (m/s) and k_s is intra-particle mass transfer coefficient (m/s).The k_{film} and k_s and associated effective and Knudsen diffusivities were estimated from empirical correlations[55]. Adsorber column pressure drop for pump power consumption was estimated with the Ergun equation [56]. For a desorber column, it was assumed that regenerant had 0% glucose entering. A 96% regeneration yield in the desorber was assumed using 90°C hot water with 4%NaOH, 0.3% oxidant, and 0.1% surfactant [57]. Regeneration flow rate was assumed 25% greater than adsorber feed flow rate.

Nanofiltration

A single-stage cross-flow hollow-fiber nanofiltration unit then separated the succinate from all formate, acetate, and most lactate by exploiting both the unique divalent (2-) charge of succinate and its molecular weight and size [17]. Succinate rejection in quarternary solutions containing monovalent formate, lactate, and acetate anions was shown to be much higher than that in single-salt solution because of their facilitated transport due to Donnan effect in the presence of divalent succinate anion [17]. For the mass balance, at maximum permeate flux, the rejection coefficients were 95%, 38%, 0.01%, and -60% for succinate, lactate, acetate, and formate, respectively [17]. The quaternary mixture of 0.3 M succinate, 0.1M acetate, 0.1 M lactate, and 0.1M formate salts that corresponded to these rejection coefficients using an NF45 membrane was formulated to simulate an actual fermention medium[17]. These published values were deemed applicable for our model because the feed mixture's 0.3 M succinate concentration [17] was similar to the 0.284 M succinate concentration from our process mass balance. Similarly high succinate rejection coefficients of 97%, 95%, and 84% at 400, 300, and 200 psig trans-membrane pressures, respectively, were also previously obtained in another work and suggested that succinate rejection became increasingly less dependent on transmembrane pressure as transmembrane pressure increased [26]. Hollow-fiber modules were selected over plate-frame module because particulate plugging was a low risk. Operating conditions for recirculation flow rate, trans-membrane pressure, number and length of hollow fibers were from literature [17, 58]. Retentate bulk and gel polarization concentrations depended on succinate having highest molecular weight and concentration of all salts. Steady-state permeate flux was estimated via a gel polarization model for dissolved solutes [58]:

$$J_{nano} = k_{nano} \ln \frac{C_{gsuc}}{C_{0suc}} \quad (42)$$

where k_{nano} is succinate mass transfer coefficient (m/s), $C_{g\text{-}suc}$ is gel polarization concentration (kg/m^3), and $C_{o\text{-}suc}$ is bulk feed concentration of succinate (kg/m^3). The $C_{g\text{-}suc}$ was obtained by first plotting steady-state permeate flux as a function of trans-membrane pressure for reported succinate concentrations [17]. Natural logarithm of sodium succinate concentration was then plotted against these fluxes to yield a straight line equation where the x-intercept corresponding to $J_{nano} = 0$ at $C_g/C_o = 1$ represented the $C_{g\text{-}suc}$ of interest. The k_{mt} was determined from a j_D-factor correlation for hollow fibers and turbulent flow regime [58]. Area and power requirement was calculated as before.

Ion exchange

Nanofiltration retentate then entered one of two fixed-bed ion exchanger columns containing weak anion exchange Dowex resin to both acidify and purify the undisassociated (protonated) succinic acid from lactic acid via its greater hydrophobicity and unique divalent charge [31]. Column loading of the binary lactate and succinate mixture occurred at pH=4 above the pKa of lactic acid and below the pKa1 of succinic acid [31]. While one column was loaded, a second was regenerated with three bed volumes of 90°C water [59]. Loading and regeneration times were equal for steady-state operation. Sorption temperature exceeded 55°C to prevent crystallization of the highly concentrated succinic acid, although its adsorption efficiency on Amberlite resin is reportedly reduced at higher temperatures [60]. Ion exchange column height was the sum of SBH (Stochiometric Bed Height)[61] and LUB (Length of Unused Bed) [40]:

$$LUB = (1 - \frac{t_b}{t^*})L_1 \quad (43)$$

where L_1 is length of small-scale column (m), t_b is breakthrough time for succinic acid (s), t* is midpoint time for succinic acid (s). t_b and t* were estimated from the breakthough curves of lactic and succinic acids on Dowex resin column [31], and:

$$SBH = \frac{v_{ion} t_s}{(1-\varepsilon)\left(\frac{q_0}{c_0}\right)} \quad (44)$$

where v_{ion} is industry-acceptable ion-exchanger hydraulic loading rate based on selected column diameter (m/s), q_o/c_o is ratio of feed succinate liquid-phase concentration to Dowex sorbent succinate solid phase-concentration in equilibrium, and t_s is service time(s). A service time of 3600 seconds corresponded to 15 column-bed loading volumes when column regeneration initiated [31]. To derive q_o/c_o, a multi-component equilibria Langmuir model and constants accounting for 1-1 and 1-2 binding were used to generate equilibrium curves [31].

Crystallization

Ion exchanger eluant then entered an idealized continuous, circulating magma, stirred-tank, cooling-type MSMPR (Mixed Solution Mixed Product Removal) crystallizer to supersaturate only anhydrous 2- succinic acid from solution at pH=2 and 4°C [16]. Yield was obtained [62]:

$$Y_{cry} = S_{ow} R_h \left[C_{0suc-cry} - C_{Fsuc-cry}\left(1 + V_d - V_e\right) \right] \quad (45)$$

where Y_{cry} is maximum yield rate of crystal produced (kg/s), S_{0w} is weight of original free solvent water (kg/s), V_d is added diluent (kg/kg original free solvent water), V_e is solvent loss from evaporation (kg/kg original free solvent water), $C_{osuc\text{-}cry}$ is initial concentration of succinic acid crystal in feed (kg anhydrous succinic acid/kg free solvent water), $C_{Fsuc\text{-}cry}$ is final concentration assumed to be solubility at 4°C and pH=2 of succinic acid crystal in saturated mother liquor (kg anhydrous succinic acid/kg free solvent water), and R_h is ratio of molecular weights of hydrate and anhydrous salts. About 2% of the water in the feed was assumed evaporated. Crystal growth was size-dependent, and nucleation was mediated by both primary and secondary mechanisms from crystal-crystallizer impeller or wall collisions [63]. To estimate crystallizer volume, experimentally-derived batch kinetic expressions for succinic acid nucleation and growth rates as functions of supersaturations were available in literature [30]:

$$B = k_B \Delta c^b M_T^v N_{cry-impeller}^z \quad (46)$$

$$G = k_g \Delta c^s N_{cry-impeller}^p \quad (47)$$

However, we combined these into a more useful relative-kinetic expression:

$$B = k_n N_{cry-impeller}^h G^g M_T^j \quad (48)$$

where B is crystal nucleation rate(s^{-1}), G is crystal growth rate(s^{-1}), N is impeller speed (rps), M_T is magma density (kg succinic acid crystal/m^3 mother liquor), and k_n, k_g k_B, h, s, j, b, v, z are dimensionless coefficients and exponents Assuming a power-volume ratio ε proportional to impeller speed as $\varepsilon = P/V \sim N^3$, by substitution crystallizer residence time was then estimated [63]:

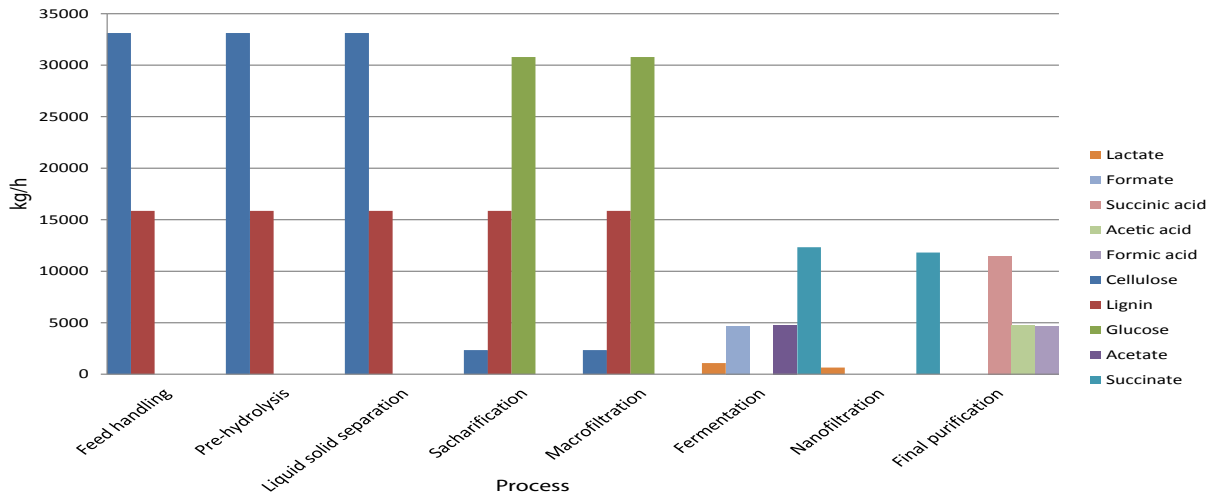

Figure 3: Changes in major stream flow rates throughout process.

Corn Stover Feed Handling	Values	Pre-Hydrolysis	Values	Blow-Down Tank	Values	Liquid-Solid Separation	Values
Temperature (°C)	40	Temperature (°C)	245	Temperature (°C)	101	Temperature (°C)	70
Pressure (atm)	1	Pressure (atm)	13.6	Pressure (atm)	1	Pressure (atm)	1
Stream ID	Flow rate (kg/hr)	Stream ID	Flow rate (kg/hr)	Stream ID	Flow rate (kg/hr)	Stream ID	Flow rate (kg/hr)
1	88542	5	137565	8	295139	10	256479
2	15625	6	3250	9	38660	11	148758
3	12042	7	154324			12	312095
4	45440						
Slurring Tank	Values	Sacharification	Values	Lignin Microfiltration	Values	Centrifugation	Values
Temperature (°C)	65	Temperature (°C)	65	Temperature (°C)	65	Temperature (°C)	65
Pressure (atm)	1	Pressure (atm)	1	Pressure (atm)	1.48	Pressure (atm)	1
Stream ID	Flow rate (kg/hr)	Stream ID	Flow rate (kg/hr)	Stream ID	Flow rate (kg/hr)	Stream ID	Flow rate (kg/hr)
13	93142	16	262335	17	262335	18	78004
14	564					19	37694
15	168628						
Fermentation	Values	Cell Microfiltration Stage#1	Values	Cell Microfiltration Stage#2	Values	Adsorption and Desorption	Values
Temperature (°C)	39	Temperature (°C)	39	Temperature (°C)	39	Temperature (°C)	68
Pressure (atm)	1	Pressure (atm)	1.97	Pressure (atm)	1.97	Pressure (atm)	1
Stream ID	Flow rate (kg/hr)	Stream ID	Flow rate (kg/hr)	Stream ID	Flow rate (kg/hr)	Stream ID	Flow rate (kg/hr)
20	40310	23	224641	25	144952.5	28	159377
21	184331	24	79688.5	26	79688.5	29	199287
22	224641			27	65264	30	199221
Nanofiltration	Values	2-Column Ion Exchange	Values	Crystallization	Values		
Temperature (°C)	25	Temperature (°C)	73	Temperature (°C)	4		
Pressure (atm)	20.41	Pressure (atm)	1	Pressure (atm)	1		
Stream ID	Flow rate (kg/hr)	Stream ID	Flow rate (kg/hr)	Stream ID	Flow rate (kg/hr)		
31	159310	34	51424.2	37	795		
32	99569	35	59741.3	38	39168		
33	59741	36	51424.2	39	11461		

Table 3: Major processes and associated flow rates, temperatures, and pressures.

$$L_m = 3.67\left[\frac{\varepsilon^{-3h} M_T^{1-j} \tau^{g-1}}{6 k_v \rho_c k_n}\right]^{\frac{1}{g+3}} \quad (49)$$

where τ is residence time (s), L_m is median crystal size (m), ε is power-volume ratio, k_v is succinic acid crystal rhombic shape factor [30,64], ρ_c is succinic acid crystal density (kg/m^3). Because j=1, crystal size and residence time were not functions of magma density. Also, because the growth to nucleation ratio>1 and g>j, crystal size was a function of residence time. The crystallizer did not include fines removal or crystal size classification. However, a 550 μm median crystal size was assumed and corresponded to a low 17.8% by weight adherence of residual mother liquor [63] that later affects filter cake porosity and reduce downstream rotary drum filter liquid washing costs. As for fermentor, crystallizer magma volume was estimated from volumetric flow rate and residence time.

Economic analysis

The biorefinery was considered an attractive investment only if recovery of investment period was less than 5 years. All costs were indexed for year 2010. No financial costs were included. Operating costs, investments and their adjustments by capital costs estimated from the materials of construction, etc. for sized units of operation from an ethanol biorefinery were used from literature [37]. Fixed costs were adjusted to include shift operators, shift supervisors, and yard employees for the operation of the downstream processes. The current variable cost of $60U.S./t of corn stover included harvesting, storage, transportation, and handling costs. A 10% per year depreciation rate for fixed-capital equipment with no salvage value was assumed. Sensitivity analysis was done to determine production costs when corn stover prices were $60/t and increased to $80 and $100/t, assuming a succinic acid yield of 1) that obtained in our baseline simulated process (Scenario A), 2) 15% (Scenario B), and 3) 19% (Scenario C). Current and future product market selling prices of $1/kg, $1/kg, $0.20/kg, $0.30/kg, and $40MW/h for succinic acid, acetic acid, formic acid, ethanol, and generated electricity, respectively, were used to determine annual revenues [65]. Because the targeted product was succinic acid, contributions to total production cost were assumed 60%, 5%, 5%, and 30% for succinic acid, acetic acid, formic acid, and ethanol, respectively.

Results and Discussion

An overall yield of 12.9% succinic acid, 10% ethanol, 5.4% acetic acid, 5.3% formic acid, and 0.5% lactic acid from corn stover feedstock was estimated after crystallization for the baseline process (Figure 3). The major process mass flow rates, temperatures, and pressures are depicted (Table 3). For 88542 kg/hr of corn stover feedstock, 11453 kg/hr succinic acid crystal was produced. Estimated area or volume requirements for the downstream units of operation are shown (Table 4). Simulation of microfiltration of insoluble lignin showed that area requirement decreased and pump power consumption increased with increasing recirculation rate (Figure 4). The baseline 6m/s recirculation rate consumed 123.325kW and resulted in a permeate flux of 0.0048 m/s.

Unit of Operation	Area (m^2)	Volume (m^3)
Lignin Microfiltration	6.82	-
Centrifuge	106.48	
Fermentor	-	178.40
Fermentor Cooling Jacket	46.83	-
Cell Microfiltration	765	-
Adsorber	-	25.91
Nanofiltration	6220	-
Ion Exchanger	-	17.14
Crystallizer	-	16.60

Table 4: Dimensional Requirements of Units of Operation for Simulated Baseline Process.

Using the available baseline kinetic terms of *M. succiniciproducens* for fermentation resulted in an overall succinic acid 12.9% yield that was less than the 18.65% yield from dried biomass from *C. glutamicum* [5] having unreported kinetic model parameters. However, replacing the *M. succiniciproducens* succinic acid productivity term α_{SA}=1.169 (kg/kg) with the α_{SA}=3.60 (kg/kg) reported for *A. succinogenes*, overall succinic yield nearly doubled to 25%, exceeding even the *C. glutamicum* yield. Such 25% yield using a term not of *C. glutamicum* but of the less productive *A. succinogenes* suggests improvements in both fermentation and our novel downstream recovery and purification are responsible. An optimal dilution rate of 1.20 hr^{-1} corresponding to maximum *M. succiniciproducens* volumetric succinic acid productivity of 69.23 kg m^{-3}hr^{-1} was predicted graphically (Figure 5) and compared well with the reported maximum *M. succiniciproducens* specific growth rate of 1.12hr^{-1} at a dissolved CO_2 concentration of 23.3mM [32].This optimal dilution rate then provided a baseline fermentor liquid volume of 178.29m3, liquid height of 12.69 m, and diameter of 4.23m as CFD inputs.

The extent that cooling jacket heat transfer area was linearly reduced by increasing $N_{impeller}$ from 10rpm to 200rpm at both 40°C and

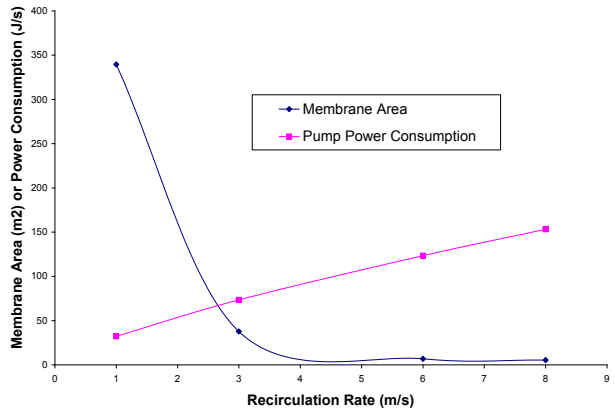

Figure 4: Lignin microfiltration membrane area and power consumption vs. recirculation rate.

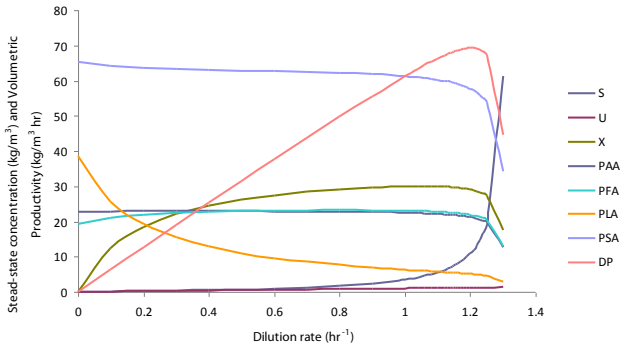

Figure 5: Graphical determination of optimal steady-states and dilution rate for M. succinoproducens fermentor.

42°C inlet temperatures were simulated (Figure 6). At inlet T_2 of 40°C, at 200rpm, CFD predicted the average liquid speed of 3.01 m/s, $P_{impeller0}$ of 433391 Watts, k_La of 0.230 s^{-1}, $[CO_{2L}]_{ss}$ of 34.9 mM, and of 19.4 m^2, $P_{impeller0}$ while at 100 rpm, CFD predicted an average liquid speed of 1.50 m/s, of 54575.3 Watts, k_La of 0.052s^{-1}, $[CO_{2L}]_{ss}$ of 33.32 mM, and of 55.4 m2. The A_{heat} appears to linearly decrease with $N_{impeller}$ with a regression coefficient of r^2=0.9896 as follows:

$$A_{heat} = -0.4291 N_{impeller} + 103.47 \quad (50)$$

The predicted $[CO_{2L}]_{ss}$ values at these conditions are within the same order of magnitude as the reported 23.3 mM when sparging with pure CO^2 at partial pressure of 101.4 kPa (y=1) in a 2.2L liquid volume fermentor at 39°C agitated at 200 rpm [32]. Assuming instead an inlet T_2 of 42°C and minimal N_0 of 10 rpm, a higher heat term $Q_{removed}$ of 869993W resulted, and CFD predicted an A_{heat} of 211.7 m^2 exceeding the available fermentor surface area of 168.6m^2. Another external heat exchanger or more efficient spiral-wound cooling coils are therefore necessary for cooling at these impeller and inlet temperature conditions.

The CFD fermentor flow fields simulated at 10rpm, 100rpm, and 200 rpm are visually presented (Figure 7). There is a more pronounced increase in average velocity from 10-100 rpm than from 100-200 rpm. At 200 rpm, using instead a graphical power number correlation for power consumption, heat transfer area increases with impeller diameter up to an asymptotic value of 48m^2 corresponding to the impeller diameter of 2m (Figure 8). The CFD fermentor flow field simulated at 200rpm for both baseline 178m3 and a 78m^3 fermentor are visually presented (Figure 9). Maximum velocity of 16.9 m/s and 10.4 m/s is predicted for the large and small fermentor, respectively. A 3:1 height to diameter ratio was specified for our process, but future CFD simulations can instead predict hydrodynamic changes from varying fermentor height. At minimum, additional hydrostatic head from increased liquid height would impact the gas-liquid CO_2 mass transfer of rising bubble flow.

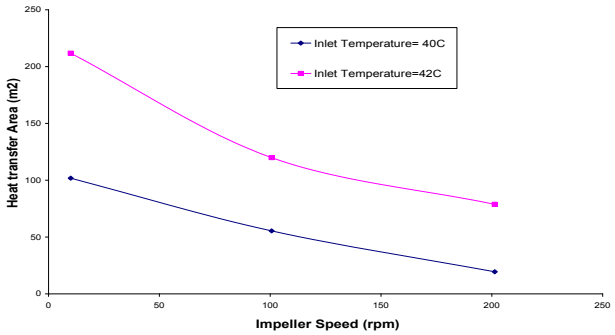

Figure 6: CFD simulation of cooling heat transfer area vs. impeller speed for 178m^3 fermentor.

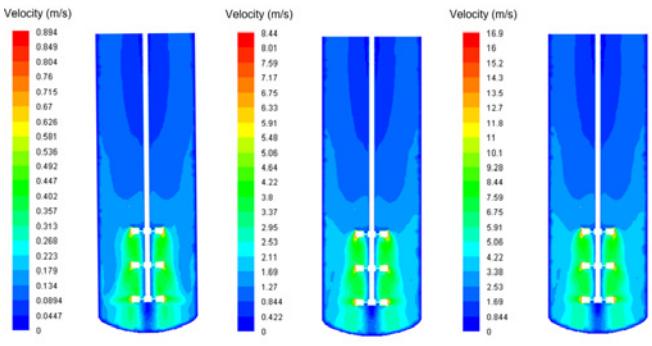

Figure 7: CFD average liquid velocity flow fields at 10, 100, and 200 rpm in 178 m^3 fermentor.

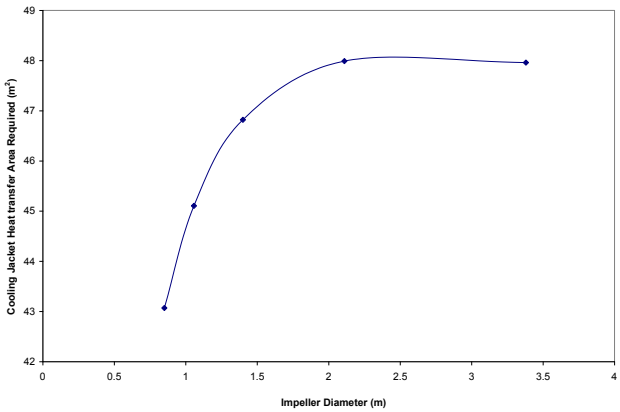

Figure 8: Cooling heat transfer area requirement vs. impeller diameter for 178m^3 fermentor.

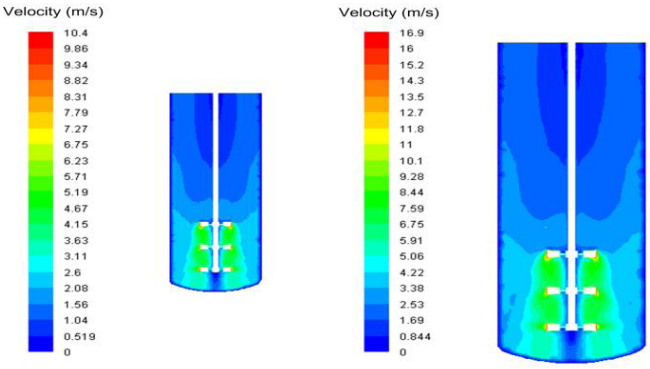

Figure 9: CFD liquid velocity flow patterns at 78m^3 and 178 m^3 fermentor volumes.

The CFD fermentor flow fields simulated at 200rpm for the smaller 78m^3 fermentor employing either the uniform impeller spacing [46] for the baseline process or a previously described alternate spacing [47] are visually presented (Figure 10). Evidently, the alternate spacing resulted in a higher maximum liquid velocity of 7.92 m/s and homogeneity and much less localized mixing, approaching more the assumed CSTR of the baseline process. Using the baseline 200 rpm and uniform impeller spacing, mixing time t_m was estimated to be 60.67 s for the 178 m^3 fermentor. With greater computational power and resources available, multi-phase CFD fermentor simulations involving sparged CO_2 gas and liquid can help process engineers optimize flow conditions and scale-up. In addition, mixing time can be used to schedule feeding of $MgCO_3$ solution to both neutralize inhibitory carboxylic acid products and provide a more soluble and storable carbon source than CO_2 gas in the fermentor [32].

Although the recycle of cells back to the fermentor after downstream microfiltration recovery was for simplicity not simulated, it is essential to note the potential outcomes if it were. The fermentation industry has long recognized the benefits of cell recycle using membranes or even expanded-bed adsorbers for increasing cell density and volumetric productivity in fermentations, and its mathematical depiction can include such things as a recycle ratio in the mass balances [66, 67]. In one study,

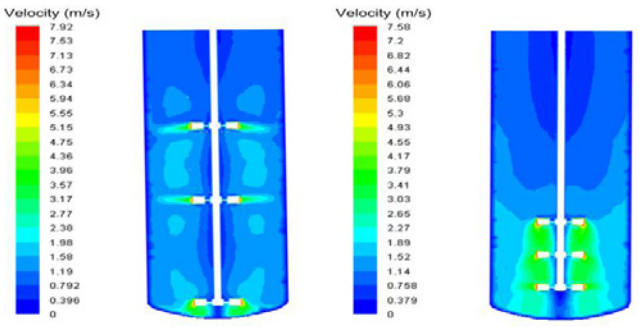

Figure 10: CFD liquid velocity flow patterns at alternating and fixed axial impeller spacing for 78m^3 fermentor.

a cell-recycled *A. succiniciproducens* fermentation achieved a high cell concentration of 6.5 g DCW /L and a three-times higher succinic acid productivity compared to batch culture, without (1) morphologically changing to an inactive spherical state at the stressful high shear rates of 800 rpm that were used to limit membrane fouling, and (2) without becoming CO_2-limited even at the highly- consuming recycled high cell densities by virtue of the concurrent supply of both pH neutralizer and inorganic carbon in the form of $NaHCO_3$ and Na_2CO_3 [68].

In another recent instance, succinic acid was produced by *Actinobacillus succinogenes sp. 130Z* in an external membrane continuous cell-recycle fermentor [67]. Compared to batch reactor, cell concentration increased three-fold to 16.4 g/L at a dilution rate 0.2 h^{-1}, and succinic acid volumetric productivity increased five-fold to 6.63 g $L^{-1}h^{-1}$ at a dilution rate of 0.5 h^{-1} [67]. At high dilution rate, contamination by a lactic acid producer and severe membrane fouling were observed [67]. *M. succiniciproducens MBEL55E* in this cell-recycle fermentor also achieved a cell concentration and succinic acid productivity at the dilution rate of 0.3 h^{-1} that were at least 3 and 2.3 times higher, respectively, compared with those at 0.1 h^{-1} dilution rate [67]. Cell concentration increased with dilution rate, even though it often oscillated before settling to a constant value [67]. Future studies to simulate the effect of such cell recycle, in addition to glucose recycle, and compare productivity gains obtained by either acid neutralization or electrodialysis removal of inhibitory acid levels, should be further done to augment the scope of this current work, as these are expected to positively impact biosuccinic acid production.

Simulation of cell microfiltration with tubes of 0.75m length and 0.007m inner diameter resulted in a total area requirement and power consumption of 876 m^2 and 78.80 kW for single-stage and a lower 765 m^2 and 68.80 kW for the two-stages of our baseline process. Because permeate flux was predicted using gel polarization theory and was a function of the ratio C_g/C_o, it was possible to have an intermediary bulk feed cell concentration C_o from the first stage that differed from that of the second stage and resulted in different permeate fluxes for each stage [53].

A primary aim of this work was to simulate a large-scale, continuous succinic acid biorefinery process. Advantages of membrane separation like microfiltration include the ability to operate without phase change, at near ambient temperatures, with relatively low energy consumption. Cross-flow microfiltration for macromolecular insoluble lignin and cells where feed flows parallel to the membrane surface was assumed more suitable for a continuous process than the relatively simpler dead-end filtration configuration requiring lower capital and maintenance costs [69], where the feed contacts the membrane surface at a perpendicular angle. This was primarily due to the intended high retentate concentrations or particle loading of insoluble lignin and cells that may otherwise rapidly compact on the filter surface as a cake layer and increase transmembrane pressure and pumping energy consumption. Also, cross-flow filtration with suitably selected membrane geometry was assumed to be less cumbersome and offer relatively more stable filtration rates and flexibility to periodically backwash or backpulse and reversibly remove some fouling, increasing long-term membrane performance and limiting membrane replacement and labor costs [69].

The *M. succiniciproducens MBEL55E* being fermented in the baseline simulated process is a rod-shaped bacteria [1]. It is again interesting to note that the morphology of this and other fermented succinic acid-producing anaerobes like *A. succinogenes* can also become more spherical and less productive for succinic acid due to high inhibitory glucose substrate concentrations above 80 g/L [70], which exceeded the calculated 10.89 g/L steady-state glucose concentration of this work. Rod-like bacterial morphology, unlike that of yeast cell layers, has in turn also influenced cake resistance differently in both dead-end and cross-flow filtration [71].

Activated carbon adsorption was previously used in downstream succinic acid recovery and purification processes [8, 26]. Simulation of the GAC adsorption column (Figure 11) resulted in an overall mass transfer coefficient of 5.29×10^{-7} m/s and pressure drop of 59 Pa/m for the baseline 841μm GAC particle diameter and a coefficient of 7.33×10^{-7} m/s and pressure drop of 90 Pa/m for a 600μm particle diameter. Evidently, greater mass transfer efficiency must be balanced with higher pump power consumption costs.

The resulting nanofiltration retentate concentrations for succinate and lactate were 197.77 and 10.85g/L, respectively, while their permeate concentrations were 3.83 and 4.12g/L, respectively. A graphical method was used to predict gel-polarization concentration for the nanofiltration unit of the baseline process (Figure 12). For this, only three data points corresponding to succinate concentrations of 0.1, 0.2, and 0.3M were available from the literature to relate permeate flux with transmembrane pressure [17] but a reasonably high R^2 value of 0.9397 was still obtained from these. A gel-polarization concentration value of 303.2 kg/m^3 succinate using the relatively simple gel-polarization model that assumes a steady-state permeate flux to be both independent of transmembrane pressure but dependent on solute concentration was calculated and then used to predict a steady-state flux of 1.42×10^{-6} m/s which was the same order magnitude but lower than the experimentally observed 4.44×10^{-6} m/s corresponding to 95% succinate rejection [17] that resulted in a very high area requirement.

Membrane nanofiltration performance depends on the complex in-

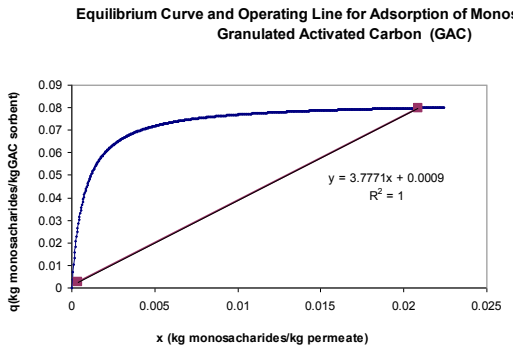

Figure 11: Adsorption equilibrium curve and operating line for glucose removal.

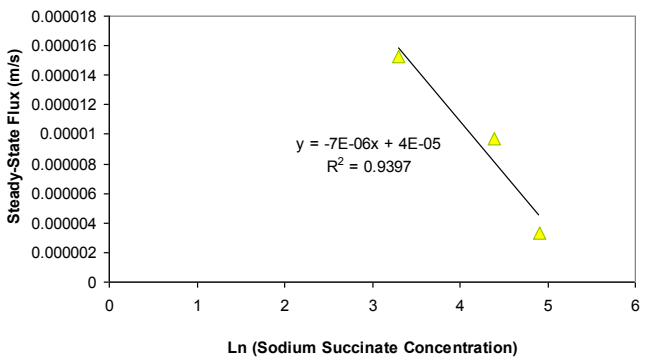

Figure 12: Estimation of gel polarization concentration for nanofiltration.

teraction of many factors, and various models have been developed to try to predict actual phenomena but do not always perfectly succeed, as the results in this study also indicate [40,42,72,73]. For instance, molecular weight, molecular size (length and width), acid disassociation constant, hydrophobicity and hydrophilicity, and diffusion coefficient were identified as key solute parameters primarily affecting solute rejection [73]. Also, molecular weight cut-off, pore size, surface charge (measured as zeta potential), hydrophobicity and hydrophilicity (measured as contact angle), and surface morphology (measured as roughness) were identified as key membrane properties primarily affecting rejection [73]. Furthermore, solute rejection was affected by feed composition, like ionic strength, pH, hardness, and organic matter [73]. Another study evaluated the effects of pH, salt concentration, and temperature on the lactate flux and rejection when using a FILMTECTM NF-200B membrane nanofiltration of concentrated organic/inorganic mixtures of salt (up to 17% (w/v)) and lactic acid (2% (w/v)). Salt rejection was low, and lactate rejection was highest at neutral pH, decreasing with temperature and salt concentration for all evaluated solutions [27]. The measured flux and rejection values indicated that skin shrinkage in concentrated salt solutions and membrane sorption of lactate influences nanofiltration beyond the typical effects of charge, solute size and osmotic difference between the retentate and permeate streams [27].

According to the literature from which the high 95% succinate rejection values for simulation were derived, divalent anions of succinate in monovalent anion solutions could also dramatically decrease the rejection of the monovalent anions of formate, lactate, and acetate in the transport through nanofiltration membranes [17]. In this previous work, flux changed with concentration even at identical pressure, and rejection of succinate by NF45 membrane for different concentrations was plotted versus transmembrane pressures and permeate [17]. The succinate rejection increased from 23 to 94% with flux and mainly depended on the flux independent of the concentration [17]. The typically observed decrease of a solute's rejection with its concentration likely due to the increased screening of membrane surface charge by counterions like sodium was not observed in the cited study because even the lowest 0.1 M concentration of Na+ tested was probably already high enough to fully screen the membrane surface charge [17]. Clearly, this current biorefinery simulation work can be improved with more comprehensive and intensive evaluation of all significant factors affecting succinate rejection in nanofiltration. Operating conditions should as a result be further optimized to exploit this technology enabling non-destructive separation of succinate from other co-products in real-life industrial processes.

Capacity, low-cost regenerability, and specificity for succinate when acidifying and purifying it were factored into the selection of Dowex MWA-1 ion exchange resin and will also be considered in more comprehensive future economic studies. Nonetheless, it was before noted that a final concentration exceeding 100 g of succinic acid/L was likely economically feasible if achieved with resins that included XUS-40285 and XFS-40422 that were similarly manufactured by Dow® [59], and, in this work, a concentration of 222.87 g of succinic acid /L was predicted. As previously mentioned, an ion exchange resin like Amberlite IR-120 that was similarly used to acidify organic salts but that, in contrast, required HCl or H_2SO_4 regeneration, was also viewed as economically favorable to electrodialysis in some instances [18]. As for the fermentor, future multi-phase CFD simulation of crystallizer involving solid succinic acid crystal and liquid mother liquor can be done to assess the effect of impeller speeds on complex crystal nucleation and growth phenomena.

The general biorefinery energy balance is shown (Table 5). Approximately 15938 kg/h of lignin was recovered via microfiltration to fuel a boiler to generate steam and electricity, and 47.9% of the corn-stover feedstock (42412 kg/hr) was not converted into products. Lignin-generated steam m_{steam} was estimated at 69410 kg/hr. However, to meet the biorefinery requirement of 154324 kg/hr of steam [37], first the steam pressure and temperature were increased by assuming instead that a commercial bubbling fluidized-bed boiler produced up to 160000 kg/h of steam at 15 MPa and T=450°C with h_{steam}=3157 kJ/kg. Second, 42% of the biomass lost in the process was assumed recovered to provide the 17863 kg/h needed to fuel this new boiler. Since the new assumed steam conditions exceeded pre-hydrolysis requirements, the steam energy content was used to produce extra electricity in a steam turbine-generator system. Assuming a total efficiency of 52%, corresponding to 65% efficiency of turbine and 80% efficiency for generator when steam pressure and temperature drop to 1.36 MPa and 245 °C, respectively, the generated power capacity was 4.2 MW, and electricity production was 36847 MWh/year. Total biorefinery power consumption, includ-

Feedstock/Product	Energy Content (MJ/h)	% of Total
Dry corn-stover biomass	1416667	100
Electricity	15120	1.1
Ethanol	141667	10
Lactic Acid	13161	0.9
Acetic Acid	153021	10.8
Formic Acid	149147	10.6
Succinic Acid	367641	26
Steam+ Hot Water	511142	36
Losses	65173	4.6

Table 5: General energy balance for succinic acid biorefinery process.

Description of Analyzed Economic Parameter	US $
Total Project Investment(installed equipment and indirect costs)	2.93E+08
Annual Fixed Operating Costs (i.e. labor, overhead)	11504720
Annual Variable Operating Costs (i.e. feedstock, cooling water, etc.)	55756068
Annual Depreciation costs	34367862
Annual Revenues (Assumes product and lignin-electricity selling prices and yields	1.75E+08
Annual Income	73207273
Return on Investment Period	4.00

Table 6: Summary of Biorefinery Economic Analysis.

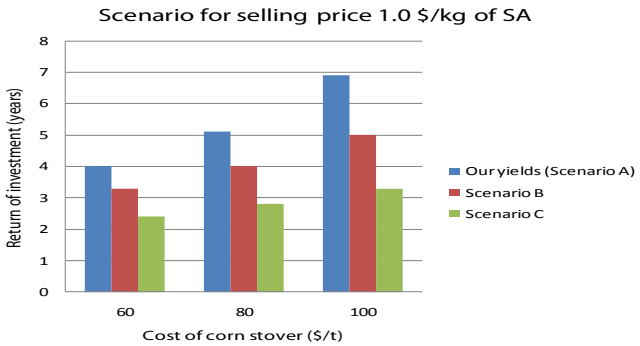

Figure 13: Periods of return of investment for succinic acid selling price of $1 U.S./kg.

ing that estimated from CFD for the fermentor, was estimated as 8561 MWh/year. The difference between energy generated and consumed (27847 MWh/year) was therefore exported to the grid for $1131420/year of revenues.

By integrating costs and capital investments literature data for ethanol biorefineries [37] with feedstock costs, product pricing, and the predicted product yields and steam generation of the baseline simulated succininc acid biorefinery process, the rough estimates of costs, revenues, and income for the baseline succinic acid bioprocess were obtained and are shown (Table 6). Corn stover raw material represented the highest variable operating cost. Assuming a $1 U.S./kg succinic acid selling price for scenarios involving our 12.9% baseline yield, 15%, and 19%, the effect of increasing corn stover costs on ROI period is summarized (Figure 13). The succinic biorefinery was therefore profitable and attractive with an ROI period of 5 years or less only if succinic acid selling exceeded $1.6/kg.

Conclusion

A novel industrial-scale biorefinery succinic acid process was described and integrated pre-treatment and hydrolysis with lignin removal and recovery to provide on-site steam and electricity generation, glucose removal and recovery, and non-destructive nanofltration succinate separation. A multi-unit process model was developed for important units of operation to enable future optimization. For the fermentor, Computational Fluid Dynamics (CFD) through its coupling to the kinetics, mass and energy balances was demonstrated to be a valuable and useful tool for scale-up. The succinic acid biorefinery was considered profitable and attractive only if the selling price of the succinic acid exceeded $1.6/kg. This work represents the first reported industrial-scale process design model for biochemically-derived succinic acid.

Acknowledgment

The work was funded by the Washington State University

Nomenclature

J_c	critical permeate flux, m/s		
ρ_p	permeate density, kg/m^3	$N_{impeller}$	rotational impeller speed, rps
μ_p	permeate viscosity, Pa*s	y	CO_2 mass fraction
r	lignin particle radius, m	d_{cell}	equivalent cell diameter,m
γ_w	tubular wall shear rate, s^{-1}	$D_{impeller}$	impeller diameter, m
$P_{micro-1}$	pump power consumption, J/s	ν_l	dynamic viscosity, m^2/s
$U_{micro-1}$	recirculation rate, m/s	c	death rate constant, m^3/s
η_p	pump efficiency	P_{SAss}	steady-state concentration of succinic acid, kg/m^3
M	impeller torque, N•m	P_{AAss}	steady-state concentration of acetic acid, kg/m^3
$d_{micro-1}$	tube inner diameter, m	P_{LAss}	steady-state concentration of lactic acid, kg/m^3
μ	specific growth rate, s^{-1}	P_{FAss}	steady-state concentration of formic acid, kg/m^3
Σ	centrifuge Sigma factor, m^2	α_{SA}	growth-associated productivity term for succinic acid, kg/kg
F	inlet/outlet volumetric flow rate, m^3/s	α_{AA}	growth-associated productivity term for acetic acid, kg/kg
X_{ss}	steady-state biomass concentration (kg DCW/m^3)	α_{LA}	growth-associated productivity term for lactic acid, kg/kg
Re	Reynolds number	α_{FA}	growth-associated productivity term for formic acid, kg/kg
X_0	feed cell biomass concentration, kg DCW/m^3	β_{SA}	non-growth associated productivity terms for succinic acid, kg/kg
V_L	fermentor liquid volume, m^3	β_{AA}	non-growth associated productivity terms for acetic acid, kg/kg
k_d	specific death rate, s^{-1}	β_{LA}	non-growth associated productivity terms for lactic acid,kg/kg
μ_{max}	maximum specific growth rate, s^{-1}	β_{FA}	non-growth associated productivity terms for formic acid, kg/kg
K_S	glucose substrate half-saturation constant, kg/m^3	S_0	glucose substrate feed concentration, kg/m^3
S_{ss}	steady-state glucose substrate concentration, kg/m^3		the inverse effective Prandtl numbers
m_s	glucose substrate maintenance term, kg/kg	$P_{impeller0}$	non-aerated impeller power consumption, J/s
$Y_{x/s}$	yield coefficient of biomass from glucose substrate, kg/kg	N_p	power number
$Y_{SA/s}$	yield coefficient of succinic acid from glucose substrate, kg/kg	μ_f	fermentation broth dynamic viscosity, Pa*s
$Y_{AA/s}$	yield coefficient of acetic acid from glucose substrate, kg/kg	t_m	mixing time, s
$Y_{LA/s}$	yield coefficient of lactic acid from glucose substrate, kg/kg	$P_{impeller\,g}$ μ	Aerated power consumption, J/s
$Y_{FA/s}$	yield coefficient of formic acid from glucose substrate, kg/kg	F_g	volumetric CO_2 flow rate, m^3/s
D	dilution rate, s^{-1}	g	gravitational constant, m^2/s
D_T	fermentor diameter, m	$H_{impeller}$	height of impeller blade, m
N_0	minimum impeller speed, rps	k_La	volumetric gas-liquid mass transfer coefficient,s^{-1}
σ	surface tension, dyne/m	v_g	superficial CO_2 gas velocity, m/s
ρ_f	fermentation broth density, kg/m^3	$F_{i_{in}}$	inlet mass flow rates of components i, kg/s
$[CO_{2L}]_{ss}$	steady-state CO_2 liquid-phase concentration, kg/m^3	$F_{i_{out}}$	outlet mass flow rates of components i, kg/s

$[CO_2]_0$	inlet CO_2 concentration, kg/m^3	$H_{i_{in}}$	inlet mass enthalpy of components i, J/kg
H	Henry's Law constant,Pa kg CO_2/m^3	$H_{i_{out}}$	outlet mass enthalpy of components i, J/kg
P	total pressure, Pa	$H_i^o(T_R)$	heat of combustion for component i, J/kg at reference temperature TR
r_{co_2}	rate of consumption of CO_2, kg/s	T_2	inlet or outlet liquid temperature, ^oC
$K_g a$	overall gas phase mass transfer coefficient, kg/Pa*s	C_{p_i}	heat capacity of component i, J kg^{-1} $^oC^{-1}$
$k_g a$	local gas phase mass transfer coefficient, kg/Pa*s	H^o_{cell}	Heat of combustion biomass enthalpy, J/kg
$[CO_2]_0$	inlet liquid-phase concentration, kg/m^3	C	weight fractions of carbon
$[CO_{2G}]_0$	inlet gas-phase concentration, kg/m^3	O	weight fractions of oxygen
$[CO_{2G}]_s$	steady-state gas-phase CO_2 concentration exiting fermentor, kg/m^3	μH	weight fractions of hydrogen
		A_{heat}	Fermentor cooloing jacket area requirement, m^2
$F_{CO2g-out}$	exiting CO_2 gas mass flow rate, kg/s	D_{cell}	particle diffusion coefficient of cells in fermentation broth, m^2/s
$F_{watervapor_{out}}$	exiting water vapor mass flow rate. kg/s	$L_{micro-2}$	tube length, m
$Q_{removed}$	rate of heat to be removed, J/s	γ	Microfiltration shear rate, s^{-1}
$\eta_{impeller}$	impeller gearbox efficiency	C_{gcel}l	gel polarization volume fraction
U	overall heat transfer coefficient, W/m2-^oC	C_{oce}ll	bulk cell volume fraction
T_C	average cooling water temperature, ^oC	q_{glu}	glucose concentration in GAC sorbent phase, mol glucose/kg GAC sorbent
T_F	fermentation broth temperature,^oC	qm	maximum sorbent capacity, mol glucose/kg GAC sorbent
h_F	heat transfer coefficient for the fermentation broth,W/m^2-^oC	Cglu	glucose concentration in liquid phase, mol glucose /m3 feed solution
h_{FD}	dirt factor from fermentation broth, W/m^2- ^oC	NTU	Number of Transfer Units
k_W	thermal conductivity of fermentor wall, J/m^2	HTU	Height of Transfer Units,m
Δx	fermentor wall thickness, m	$K_{adsorber}$	overall mass transfer coefficient, m/s
h_C	cooling water heat transfer coefficient, W/m^2-^oC	$v_{adsorber}$	Adsorber hydraulic loading rate, m/s
h_{CD}	cooling water dirt factor heat transfer coefficient, W/m^2 ^oC	a_i	particle interfacial area/volume ratio, m^{-1}
μ_W	wall viscosity, kg/s-m	SBH	stochiometric bed height,m
k_F	fermentation broth thermal conductivity, W/m-^oC	LUB	length of unused bed,m
$J_{micro-2}$	microfiltration steady-state permeate flux, m/s	L_1	length of small-scale column, m
ε	bed porosity or void fraction	t_b	breakthrough time for succinic acid, s
d_p	GAC particle diameter, m	t*	midpoint time for succinic acid, s

k_{film}	film-mass transfer coefficient, m/s	v_{ion}	ion-exchanger hydraulic loading rate, m/s
k_s	intra-particle mass transfer coefficient, m/s	q_o/c_o	ratio of feed succinate liquid-phase concentration to Dowex sorbent succinate solid phase-concentration in equilibrium
k_{nano}	succinate mass transfer coefficient, m/s	t_s	service time(s)
$C_{g\text{-}suc}$	Succinate gel polarization concentration, kg/m^3	Y_{cry}	maximum yield rate of crystal produced, kg/s
$C_{o\text{-}suc}$	bulk feed concentration of succinate, kg/m^3	S0w	weight of original free solvent water, kg/s
J_{nano}	nanofiltration steady-state permeate flux, m/s	V_d	added diluent, kg/kg original free solvent water
R_h	ratio of molecular weights of hydrate and anhydrous salts	V_e	solvent loss from evaporation, kg/kg original free solvent water
B	crystal nucleation rate, s^{-1}	$C_{osuc\text{-}cry}$	initial concentration of succinic acid crystal in feed, kg anhydrous succinic acid/kg free solvent water
G	crystal growth rate, s^{-1}	$C_{Fsuc\text{-}cry}$	final concentration of succininc acid in saturated mother liquor, kg anhydrous succinic acid/kg free solvent water
N_{cry}	crystallizer impeller speed (rps)	z	Crystallizer exponent
M_T	magma density, kg succinic acid crystal/m3 mother liquor	v	Crystallizer exponent
k_n	Crystallizer coefficient	b	Crystallizer exponent
k_g	Crystallizer coefficient	j	Crystallizer exponent
k_B	Crystallizer coefficient	s	Crystallizer exponent
L_m	median crystal size, m	h	Crystallizer exponent
τ	Crystallizer residence time (s)	k_v	succinic acid crystal rhombic shape factor
ε	power-volume ratio	ρ_c	succinic acid crystal density, kg/m$_3$
Δc	supersaturation, kg/m$_3$	$A_{micro-1}$	Area requirement (m^2)

References

1. Song H, Lee SY (2006) Production of succinic acid by bacterial fermentation. Enzyme and Microbial Technology 39: 352-361.
2. Zeikus JG, Jain MK, Elankovan P (1999) Biotechnology of succinic acid production and markets for derived industrial products. Appl Microbiol Biotechnol 51: 545-552.
3. Beauprez JJ, De Mey M, Soetaert WK (2010) Microbial succinic acid production: Natural versus metabolic engineered producers. Process Biochemistry 45: 1103-1114.
4. Lynd LR, Wyman C, Laser M, Johnson D, Landucci R (2005) Strategic biorefinery analysis: Analysis of biorefineries. NREL Subcontractor Report SR-510-35578 National Renewable Energy Laboratory: Golden, Colorado.
5. Luo L, van der Voet E, Huppes G (2010) Biorefining of lignocellulosic feedstock - Technical, economic and environmental considerations. Bioresource Technology 101: 5023-5032.
6. Song H, Jang SH, Park JM, Lee SY (2008) Modeling of batch fermentation kinetics for succinic acid production by Mannheimia succiniciproducens. Biochemical Engineering Journal 40: 107-115.
7. Werpy T, Petersen G, Aden A, Bozell J, Holladay J, et al. (2004) Top value added chemicals from biomass. Volume I, Pacific Northwest National Laboratory, Richland, Washington.
8. Lin SKC, Du C, Blaga AC, Camarut M, Webb C, et al. (2010) Novel resin-based

vacuum distillation-crystallisation method for recovery of succinic acid crystals from fermentation broths. Green Chem 12: 666-671.

9. McCoy M (2009) Big plans for succinic acid. Chemical & Engineering News 87: 23-25.
10. Elbert J (2007) The quest to commercialize biobased succinic-acid. Biomass Magazine.
11. Yu J, Li ZM, Ye Q, Yang Y, Chen SL (2010) Development of succinic acid production from corncob hydrolysate by Actinobacillus succinogenes. Journal of Industrial Microbiology & Biotechnology 37: 1033-1040.
12. Luque R, Lin CSK, Du C, Macquarrie DJ, Koutinas A, et al. (2009) Chemical transformations of succinic acid recovered from fermentation broths by a novel direct vacuum distillation-crystallisation method. Green Chem 11: 193-200.
13. Song H, Huh YS, Lee SY, Hong WH, Hong YK (2007) Recovery of succinic acid produced by fermentation of a metabolically engineered Mannheimia succiniciproducens strain. J Biotechnol 132: 445-452.
14. Li J, Zheng XY, Fang XJ, Liu SW, Chen KQ, et al. (2011) A complete industrial system for economical succinic acid production by Actinobacillus succinogenes. Bioresource Technology 102: 6147-6152.
15. Huh YS, Jun YS, Hong YK, Song H, Lee SY, et al. (2006) Effective purification of succinic acid from fermentation broth produced by Mannheimia succiniciproducens. Process Biochemistry 41: 1461-1465.
16. Li Q, Wang D, Wu Y, Li W, Zhang Y, et al. (2010) One step recovery of succinic acid from fermentation broths by crystallization. Separation and Purification Technology 72: 294-300.
17. Kang SH, Chang YK (2005) Removal of organic acid salts from simulated fermentation broth containing succinate by nanofiltration. Journal of Membrane Science 246: 49-57.
18. Wang Y, Huang C, Xu T (2011) Which is more competitive for production of organic acids, ion-exchange or electrodialysis with bipolar membranes? Journal of Membrane Science 374: 150-156.
19. Meynial-Salles I, Dorotyn S, Soucaille P (2008) A new process for the continuous production of succinic acid from glucose at high yield, titer, and productivity. Biotechnology and Bioengineering 99: 129-135.
20. Huang C, Xu T, Zhang Y, Xue Y, Chen G (2007) Application of electrodialysis to the production of organic acids: State-of-the-art and recent developments. Journal of Membrane Science 288: 1-12.
21. Lee EG, Kang SH, Kim HH, Chang YK (2006) Recovery of lactic acid from fermentation broth by the two-stage process of nanofiltration and water-splitting electrodialysis. Biotechnology and Bioprocess Engineering 11: 313-318.
22. Glassner DA, Elankovan P, Beacom DR, Berglund KA (1995) Purification process for succinic acid produced by fermentation. Applied Biochemistry and Biotechnology 52: 73-82.
23. Alvarez F, Alvarez R, Coca J, Sandeaux J, Sandeaux R, et al. (1997) Salicylic acid production by electrodialysis with bipolar membranes. Journal of Membrane Science 123: 61-69.
24. Glassner DA (1992) Process for the production and purification of succinic acid. US Patent 5,143,834.
25. Wang Y, Zhang X, Xu T (2010) Integration of conventional electrodialysis and electrodialysis with bipolar membranes for production of organic acids. Journal of Membrane Science 365: 294-301.
26. Nghiem N, Davison BH, Donnelly MI, Tsai SP, Frye JG (2001) An integrated process for the production of chemicals from biologically derived succinic acid. ACS Symposium Series 784: 160-173.
27. Freger V, Arnot TC, Howell JA (2000) Separation of concentrated organic/inorganic salt mixtures by nanofiltration. Journal of Membrane Science 178: 185-193.
28. Gineste JL, Pourcelly G, Lorrain Y, Persin F, Gavach C (1996) Analysis of factors limiting the use of bipolar membranes: A simplified model to determine trends. Journal of Membrane Science 112:199-208.
29. Zondervan, E, Nawaz M, de Haan AB, Woodley JM, Gani R (2011) Optimal design of a multi-product biorefinery system. Computers & Chemical Engineering 35: 1752-1766.
30. Qiu Y, Rasmuson AC (1991) Nucleation and Growth of Succinic Acid in a Batch Cooling Crystallizer. AiChE Journal 37: 1293-1304.
31. Husson SM, King CJ (1999) Multiple-acid equilibria in adsorption of carboxylic acids from dilute aqueous solution. Ind Eng Chem Res 38: 502-511.
32. Song H, Lee JW, Choi S, You JK, Hong WH, et al. (2007) Effects of dissolved CO2 levels on the growth of Mannheimia succiniciproducens and succinic acid production. Biotechnology and Bioengineering 98: 1296-1304.
33. Lin SKC, Du C, Koutinas A, Wang R, Webb C (2008) Substrate and product inhibition kinetics in succinic acid production by Actinobacillus succinogenes. Biochemical Engineering Journal 41: 128-135.
34. Blanch HW, Clark DS (1997) Biochemical Engineering. New York Marcel Dekker, Inc.
35. Harris CK, Roekaerts D, Rosendal FJJ, Buitendijk FGJ, Daskopoulos P, et al. (1996) Computational fluid dynamics for chemical reactor engineering. Chemical Engineering Science 51: 1569-1594.
36. Fluent F (2006) 6.3 User's Guide. Fluent, Inc.: Lebanon, NH.
37. Aden A, Ruth M, Ibsen K, Jechura J, Neeves K, et al. (2002) Lignocellulosic biomass to ethanol process design and economics utilizing co-current dilute acid prehydrolysis and enzymatic hydrolysis for corn stover. NREL Technical Report, National Renewable Energy Laboratory: Golden, Colorado.
38. Sadrameli SM, Seames W, Mann M (2008) Prediction of higher heating values for saturated fatty acids from their physical properties.Fuel 87: 1776-1780.
39. Wallberg O (2005) Design of Ultrafiltration Process for Extraction of Lignin from Kraft black liquor. Internal Report, Department of Chemical Engineering, Lund Institute of Technology, Sweden: 1-9.
40. Harrison RG, Todd P, Rudge SR, Petrides DP (2003) Bioseparations Science and Engineering. Oxford: Oxford University Press.
41. Field RW, Pearce GK (2011) Critical, sustainable and threshold fluxes for membrane filtration with water industry applications. Advances in Colloid and Interface Science 164: 38-44.
42. Mulder M (1996) Basic Principles of Membrane Technology (2ndedn), Klumer Academic Publishers.
43. Zheng P, Fang L, Xu Y, Dong JJ, Ni Y, et al. (2010) Succinic acid production from corn stover by simultaneous saccharification and fermentation using Actinobacillus succinogenes. Bioresource Technology 101: 7889-7894.
44. van't Riet K, Tramper J (1991) Basic Bioreactor Design. New York: Marcel Dekker, Inc.
45. Lange H, Taillandier P, Riba JP (2001) Effect of high shear stress on microbial viability. J Chem Technol Biotechnol 76: 501-505.
46. Lee JM (1992) Biochemical Engineering. Prentice-Hall, Inc.
47. Paul EL, Atiemo-Obeng VA, Kresta SM (2004) Handbook of industrial mixing-Science and Practice.
48. Versteeg HK, Malalasekera W (1995) An Introduction to Computational Fluid Dynamics, Harlow, England: Addison Wesley Longman Limited.
49. Antoine C (1888) Tensions des vapeurs; nouvelle relation entre les tensions et les températures. Comptes Rendus des Séances de l'Académie des Sciences 107: 681–684, 778–780, 836–837.
50. Diosady LL, Puzanov T (2005) Membrane Fermentation of Lactic Acid. International Journal of Applied Science and Engineering 3: 19-25.
51. Song L (1998) Flux decline in crossflow microfiltration and ultrafiltration: mechanisms and modeling of membrane fouling. Journal of Membrane Science 139: 183-200.
52. Song L (1998) A new model for the calculation of the limiting flux in ultrafiltration. Journal of Membrane Science 144: 173-185.
53. Coulson JM, Richardson JF (1991) Chemical Engineering (4thedn) Vol 2, Butterworth Heinemann.
54. Lee JW, Kwon TO, Moon IS (2004) Adsorption of mono saccharides, disaccharides, and maltooligosaccharides on activated carbon for separation of maltopentaose. Carbon 42: 371-380.
55. Uchida H, Iwai Y, Amiya M, Arai Y (1997) Adsorption behaviors of 2,6- and 2,7

dimethylnaphthalenes in supercritical carbon dioxide using NaY-type zeolite. Ind Eng Chem Res 36: 424-429.

56. Knaebel KS (1990) A"How-To" Guide for Adsorber Design. Adsorption Research, Inc., Dublin, Ohio.

57. Sun K, Jiang JC, Xu JM (2009) Decolorization and chemical regeneration of granular activated carbon used in citric acid refining. Bull Chem Soc Ethiop 23: 29-36.

58. Ladisch MR (2001) Bioseparations Engineering. Principles, Practice, and Economics. John Wiley & Sons, Inc.

59. Davison BH, Nghiem NP, Richardson GL (2004) Succinic acid adsorption from fermentation broth and regeneration. Applied Biochemistry and Biotechnology 114: 653-669.

60. Nam HG, Park KM, Lim SS, Mun S (2011) Adsorption Equilibria of Succinic Acid and Lactic Acid on Amberchrom CG300C Resin. J Chem Eng Data 56: 464-471.

61. Cooney DO (1998) Adsorption design for wastewater treatment CRC Press, LLC.

62. Tavare NS (1994) Industrial Crystallization: Process Simulation Analysis and Design. Plenum Press, New York.

63. Jancik SJ, Grootscholten PAM (1984) Industrial Crystallization. Delft University Press.

64. Mullin JW, Whiting MJL (1980) Succinic Acid Crystal-Growth rates in aqueous-solution. Ind Eng Chem Fundamen 19: 117-121.

65. Chang, J (2011) Indicative Chemical Prices A-Z, ICIS Chemical Business 2011.

66. Park TH, Juan H, Lim HC (1991) Theoretical-analysis of the effect of cell recycling on recombinant cell fermentation processes. Biotechnol Prog 7: 77-84.

67. Kim MI, Kim NJ, Shang L, Chang YK, Lee SY (2009) Continuous production of succinic acid using an external membrane cell recycle system. Journal of Microbiology and Biotechnology 19: 1369-1373.

68. Lee PC, Lee SY, Chang HN (2008) Cell recycled culture of succinic acid-producing Anaerobiospirillum succiniciproducens using an internal membrane filtration system. Journal of Microbiology and Biotechnology 18: 1252-1256.

69. Mhurchú JN (2008) Dead-end and crossflow microfiltration of yeast and bentonite suspensions: experimental and modelling studies incorporating the use of artificial neural networks, PhD thesis, School of Biotechnology, Dublin City University: Dublin, 1-243.

70. Corona-Gonzalez RI, Bories A, Gonzalez-Alvarez V, Pelayo-Ortiz C (2008) Kinetic study of succinic acid production by Actinobacillus succinogenes ZT-130. Process Biochemistry 43: 1047-1053.

71. Mota M, Teixeira JA, Yelshin A (2002) Influence of cell-shape on the cake resistance in dead-end and cross-flow filtrations. Separation and Purification Technology 27:137-144.

72. Koyuncu I, Topacik D (2002) Effect of organic ion on the separation of salts by nanofiltration membranes. Journal of Membrane Science 195: 247-263.

73. Bellona C, Drewes, JE, Xu P, Amy G (2004) Factors affecting the rejection of organic solutes during NF/RO treatment - a literature review. Water Research 38: 2795-2809.

This article was originally published in a special issue, **Bioprocessing** handled by Editor(s). Dr. Mark R. Wilkins, Oklahoma State University, USA; Stefano Curcio, University of Calabria, Italy